Mathematical Modelling of PI3K/Akt Pathway in Microglia

Alireza Poshtkohi[1*], John Wade[2], Liam McDaid[2], Junxiu Liu[2], Mark L Dallas[3], Angela Bithell[3]

[1] School of Physics, Engineering and Computer Science, University of Hertfordshire, Hatfield, Hertfordshire, United Kingdom

[2]School of Computing, Engineering and Intelligent Systems, University of Ulster, Londonderry, United Kingdom

[3] School of Pharmacy, University of Reading, Reading, United Kingdom

Email addresses: a.poshtkohi@herts.ac.uk; {jj.wade, lj.mcdaid, j.liu16}@ulster.ac.uk; {m.dallas, a.bithell}@reading.ac.uk

Abstract

The motility of microglia involves intracellular signalling pathways that are predominantly controlled by changes in cytosolic Ca^{2+} and activation of PI3K/Akt (phosphoinositide-3-kinase/protein kinase B). Herein, we develop a novel biophysical model for cytosolic Ca^{2+} activation of the PI3K/Akt pathway in microglia where Ca^{2+} influx is mediated by both P2Y purinergic receptors (P2YR) and P2X purinergic receptors (P2XR). The model parameters are estimated by employing optimisation techniques to fit the model to phosphorylated Akt (pAkt) experimental modelling/*in vitro* data. The integrated model supports the hypothesis that Ca^{2+} influx via P2YR and P2XR can explain the experimentally reported biphasic transient responses in measuring pAkt levels. Our predictions reveal new quantitative

insights into P2Rs on how they regulate Ca^{2+} and Akt in terms of physiological interactions and transient responses. It is shown that the upregulation of P2X receptors through a repetitive application of agonist results in a continual increase in the baseline [Ca^{2+}] which causes the biphasic response to become a monophasic response which prolongs elevated levels of pAkt.

Keywords: human microglia, calcium signalling, purinergic P2Y receptor, IP_3 receptor, PI3K/Akt pathway, mathematical modelling

1. Introduction

Microglia play a key role in the central nervous system (CNS) and have attracted wide attention because of their contribution to brain physiology and pathology (Erb, Woods, Khalafalla, & Weisman, 2019; Hickman, Izzy, Sen, Morsett, & El Khoury, 2018; Kettenmann, Hanisch, Noda, & Verkhratsky, 2011; Thei, Imm, Kaisis, Dallas, & Kerrigan, 2018; Wolf, Boddeke, & Kettenmann, 2017). Microglia are highly dynamic and plastic cells that display multivariant morphological and functional states (Franco-Bocanegra, McAuley, Nicoll, & Boche, 2019; Madry & Attwell, 2015; Paolicelli et al., 2022). To maintain this dynamic state, restructuring of the actin cytoskeleton consists of a complex molecular cascade that involves a set of membrane-resident ion-coupled receptors (Madry & Attwell, 2015). These receptors enable microglia to sense local ionic and chemical concentration changes to begin either process extension or whole-cell chemotaxis. Ca^{2+} is a key signal transduction cation acting as a pivotal second messenger in microglial motility. Crucial for microglia motility are purinergic receptors, specialised ATP-gated ion channels exhibiting relatively high calcium

permeability, two types of which known as P2X and P2Y family of receptors have been extensively implicated in microglia Ca^{2+} dynamics. Specifically, $P2X_1$, $P2X_4$ and $P2X_7$ receptors from the P2X family, and $P2Y_2$, $P2Y_6$ and $P2Y_{12\text{-}14}$ from the P2Y family of receptors have been identified in microglial activity (Brawek & Garaschuk, 2013; Honda et al., 2001; Kettenmann et al., 2011; Ohsawa et al., 2007; Umpierre, Bystrom, Ying, Liu, & Wu, 2019; Younger, Murugan, Rao, Wu, & Chandra, 2019). For example, process extension in microglia is regulated by the activation of the $P2Y_{12}$ receptor and changes in $[Ca^{2+}]_i$ and the subsequent activation of the PI3K (phosphoinositide-3-kinase) pathway (Irino, Nakamura, Inoue, Kohsaka, & Ohsawa, 2008).

The involvement of extracellular adenine nucleotides is a crucial part of understanding P2X and P2Y receptor signalling in the CNS because a wide spectrum of microglial receptors are mediated directly by extracellular nucleotides (Yegutkin, 2014). One important ligand to control the level of Ca^{2+} in the intracellular space is ATP by directly activating the ligand-gated P2X receptors in eukaryotic cells (North, 2016) and human microglia (Poshtkohi et al., 2021). After ATP binding, a channel pore opens and facilitates Ca^{2+}, Na^{+} and K^{+} to traverse across the cell membrane. It has been shown that ionic fluxes regulated by P2XR activation participate in triggering the PI3K pathway through Ca^{2+} uptake from the extracellular space (Domercq, Vazquez, & Matute, 2013; Ohsawa et al., 2007). The $P2Y_{12}$ receptor is a G protein-coupled receptor and is triggered by ATP and ADP molecules (Cattaneo, 2015). Its activation gives rise to Ca^{2+} release from intracellular stores, particularly the endoplasmic reticulum, which then stimulates CRAC (calcium release-activated channel) channels for an influx of Ca^{2+} to compensate the intracellular stores and additionally opens $K_{Ca}3.1$ channels for efflux of K^{+} [18]. These complex events activate PI3K and PLC pathways, which subsequently result

in the phosphorylation of Akt. pAkt promotes process extension and chemotaxis by reorganisation of the actin cytoskeleton [19].

Mathematical biology is an overarching enabling technology that bridges the gap between reported experiments and unexplored cell behaviours. Many mathematical models have been proposed for modelling the PI3K/Akt pathway, metabotropic receptors and IP_3Rs in cell types other than microglia. Here, we briefly review a number of existing biophysical models that are relevant to this study.

One of the pioneering IP_3R models involves channel activation and deactivation via Ca^{2+} and is an eight-state Markov model which assumes the receptor is made up of three individual subunits (De Young & Keizer, 1992). Each subunit has two Ca^{2+} binding sites for activation and inactivation and an IP_3 binding site. The model can be reduced further by several simplifying assumptions (Li & Rinzel, 1994). Because IP_3 and Ca^{2+} bind quickly to their activating binding sites, it can be assumed that the dynamics of the states regarding these sites are negligible and thus the receptor works in a quasi-steady state. This results in a simplified Hodgkin–Huxley-style model with two-state variables. A type-2 IP_3 receptor model using Markov states in (Sneyd & Dufour, 2002) is presented because other models do not comply with the transient responses of the receptor observed experimentally.

The $P2Y_2$ receptor (Greg Lemon, 2003; G Lemon, Gibson, & Bennett, 2003) was modelled by constructing a complex reaction network for the G-protein cascade, which is activated by uridine triphosphate (UTP). The model takes transient responses of Ca^{2+}, IP_3 and PIP_2 into consideration. Equilibrium assumptions are incorporated into the model to derive simpler equations, but they may not be applied to other cells because every cell has different

transient responses. A mathematical model that has been derived from an 8-state Markov model is reused for the IP_3 receptor proposed by Li and Rinzel (Li & Rinzel, 1994).

In (Song & Varner, 2009), a mathematical model for P2-mediated calcium signalling in sensory neurons is developed by using basic kinetic reactions. The model, adopted from (Dolan & Diamond, 2014; Mishra & Bhalla, 2002; Purvis, Chatterjee, Brass, & Diamond, 2008; Shakhidzhanov, Shaturny, Panteleev, & Sveshnikova, 2015), includes signalling pathways regulating receptor activity and G-protein cascade and yields transient cytosolic Ca^{2+} changes by reusing a model of the IP_3 receptor (Sneyd & Dufour, 2002). The model is extremely complicated because of 90 species, 252 unknown parameters and 93 biochemical reactions. Because of the complexity, the authors used 9 different data sets for different cells to estimate the model parameters but were unable to find unique parameters. A multi-objective optimisation algorithm (Ensemble Simulated Annealing) was instead employed to find near-optimal parameters.

Directed microglial motility through Akt requires a complex family of intracellular signalling pathways over which multi-component signalling, feedback and cross-talks take place. A multi-step process controls Akt activation by involving PI3K. Therefore, developing a mathematical model for such a complex pathway to understand its regulation in microglia is challenging. Parameter estimation of this biological model also becomes difficult because of the large number of model parameters that must be estimated. Consequently, several computational models of the PI3K/Akt signalling pathway have been reported in pursuit of finding therapeutic targets for various diseases (Hatakeyama et al., 2003; Ji et al., 2020; Koh, Teong, Clément, Hsu, & Thiagarajan, 2006; Pappalardo et al., 2016; Tan, Popel, & Mac

Gabhann, 2013). The complexity of these models arises from the large number of ordinary differential equations (ODEs) and model parameters.

This paper aims to develop a biophysical model of ADP-meditated $P2Y_{12}R$ and P2XR-mediated Ca^{2+} influx in microglia. The model is then used to study pAkt activity via the PI3K/Akt/CaMKII pathway. Due to the complexity of the existing models and the lack of adequate experimental data, this paper proposes a simpler model that captures published microglial Ca^{2+} and pAkt experimental data. This model is then used to make predictions regarding Ca^{2+}/pAkt dynamics in microglia.

2. Methods

$P2Y_{12}$ is an important receptor that is reported to be actively responsible for directed motility and chemotaxis (Madry & Attwell, 2015). In this section, a biophysical model for the time courses of Ca^{2+} and pAkt in the cytosol is developed. Fig. 1 portrays a high-level view of the components integrated into the model. In this article, it is hypothesised that $P2Y_{12}R$ in microglia is associated with $G_{\alpha i}$-GPCR signalling which triggers intracellular calcium transients as it has been experimentally shown that this receptor is involved with a (yet unknown) PLC (phospholipase C) pathway (Irino et al., 2008). Of course, more work in the future is needed to test this hypothesis because, in contrast, the $P2Y_{12}$ receptor can couple to the $G_{\alpha i}$ subunit in platelets and give rise to only adenyl cyclase inhibition and a cAMP decrease without meditating Ca^{2+} (Koupenova & Ravid, 2018). The $P2Y_{12}$ receptor first activates PLC which then converts phosphatidylinositol 4,5-bisphosphate (PIP_2) which in turn leads to the creation of inositol 1,4,5-trisphosphate (IP_3) as an intracellular second messenger. IP_3 activates the IP_3R on the endoplasmic reticulum leading to Calcium Induced

Calcium Release (CICR). IP_3 and other signalling intermediates are recycled perpetually by a set of signalling events such as phosphorylation and dephosphorylation reactions. Diacylglycerol (DAG) is generated by PLC_β and affects PKC activity through the intracellular Ca^{2+}.

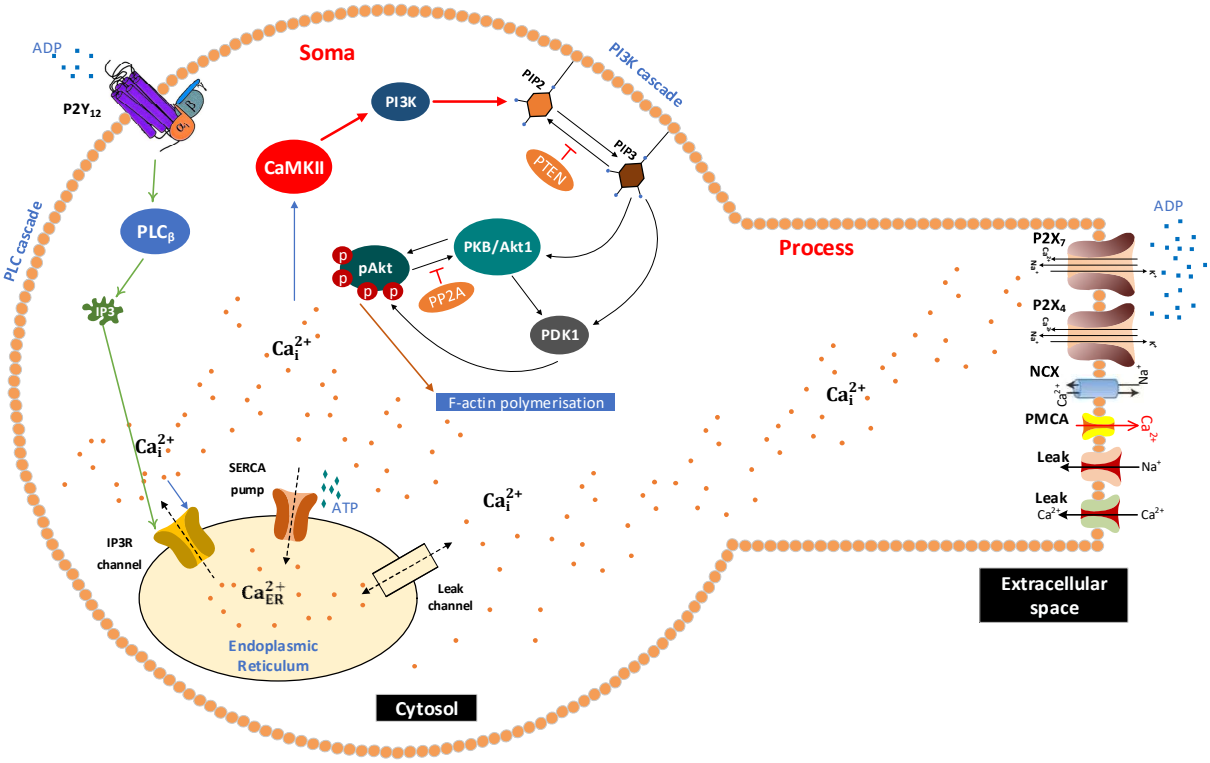

Figure 1: A model of $P2Y_{12}$-mediated calcium and PI3K/Akt signalling pathways of a microglial cell involved in chemotaxis (directed motility). The $P2Y_{12}$ receptor is activated after ADP binding and phospholipase C (PLC) is evoked. PLC hydrolyses PIP_2 into IP_3 and DAG. IP_3R channels are open when IP_3 and intracellular Ca^{2+} bind simultaneously and Ca^{2+}_{ER} is released from the endoplasmic reticulum (ER) into the cytoplasmic region. The PI signalling network recycles phosphorylated phosphatidylinositol (PI) substances while the SERCA (Sarco/endoplasmic reticulum Ca^{2+}-ATPase) and leak channel function as major

transporters of calcium from the cytosol into the ER. In the microglia process, P2XRs, the Na^+/Ca^{2+} exchanger (NCX) and the plasma membrane Ca^{2+}-ATPase (PMCA) along with Ca^{2+} and Na^+ leakage channels facilitate the influx of Ca^{2+} from the extracellular space, which subsequently diffuses into the somatic space. Aggerated Ca^{2+} in the soma phosphorylates CaMKII (Ca^{2+}/calmodulin-dependent protein kinase II). The elevated level of CaMKII in turn directly activates the PI3K/Akt pathway. pAkt production is regulated by a complex network of potentiators like PDK1 (pyruvate dehydrogenase kinase 1), inhibitors like PTEN (phosphatase and tensin homolog) and species convertors.

The PI3K/Akt signalling pathway is not well understood. However, from the literature (Fan, Xie, & Chung, 2017; Kölsch, Charest, & Firtel, 2008; Sasaki & Firtel, 2006), a complex signalling pathway can be constructed as shown in Fig 1. It appears that either ADP or ATP can activate the G protein-coupled receptor (GPCR), $P2Y_{12}$ (Irino et al., 2008; Ohsawa et al., 2007), which directly leads to the production of PIP_3 from PIP_2 by the $G_{\beta\gamma}$ subunit. The $G_{\beta\gamma}$ subunit simultaneously triggers the PLC_β pathway (resulting in a rapid rise of cytosolic [Ca^{2+}] (Madry & Attwell, 2015)) and indirectly controls the conversion of PIP_2 to PIP_3 during phosphorylation (i.e. PLC_β converts PIP_2 to IP_3 and so can slow down the rate at which PIP_2 is turned into PIP_3 by $PI3K_\gamma$) while PTEN inhibits PIP_3. The total generated PIP_3 leads to the activation of Akt (followed by the generation of pAkt) which in turn directly takes part in F-actin polymerisation. Unfortunately, there is limited experimental data for the PI3K/Akt pathway in microglial cells. However, experimental data does exist relating intracellular

[Ca^{2+}] and pAkt to extracellular ADP in rat primary cultured microglia. This data will serve to validate the proposed model.

There is growing evidence in the literature that both P2X and P2Y receptors are involved in the directed motility of microglia by activation of the PI3K/Akt pathway (Jacques-Silva et al., 2004; Ohsawa et al., 2007; Tsuda, Toyomitsu, Kometani, Tozaki-Saitoh, & Inoue, 2009). Additionally, it is well known that the $P2Y_{12}$ receptor activates the PI3K/Akt pathway via underlying GPCR signalling (Andrews, Stephens, & Hawkins, 2007; Dorsam & Kunapuli, 2004; Gurbel, Kuliopulos, & Tantry, 2015; Sasaki & Firtel, 2006). A biphasic response has been reported as described in the next sections, two peaks displaying different temporal profiles exist in pAkt experimental data in microglia. This paper proposes that the P2Y receptor regulates the first peak, whereas the second peak is regulated by P2X receptors. Specifically, these receptors activate two sources of Ca^{2+} influx which contribute to the total cytosolic Ca^{2+} where one source of Ca^{2+} is from the endoplasmic reticulum (ER), and the second is via the P2XR, which subsequently diffuses to the microglia soma: the delay associated with diffusion is modelled using a fixed delayed time. Furthermore, there is extensive evidence that P2X receptors are located on the processes of glial cells (Ashour & Deuchars, 2004) which is consistent with the compartmental model in Fig. 1 for supporting the idea of a diffusion time delay arising from P2X receptors. To better quantify this hypothesis, supplementary material (S1) shows that when P2XRs are switched off the model can only cover a single peak thereby biophysically implying the presence of both P2YR and P2XR-mediated responses through mathematical modelling. In the proposed model, CaMKII (Ca^{2+}/calmodulin-dependent protein kinase II) is phosphorylated by the elevated Ca^{2+}

concentration in the microglia soma which directly activates the PI3K/Akt pathway (Agell, Bachs, Rocamora, & Villalonga, 2002; Jing et al., 2016; Yano, Tokumitsu, & Soderling, 1998).

2. 1. Proposed Model

In this section, a biophysical model that relates the influx of Ca^{2+}, via P2XR and P2YR, to pAkt activation is developed. An existing model (Wade, McDaid, Harkin, Crunelli, & Kelso, 2012) is used for IP_3 generation and degradation in terms of a single ordinary differential equation where the binding of ADP to the $P2Y_{12}$ receptor releases IP_3 according to Eq. 1 below.

$$\frac{dIP_3{}^{ADP}}{dt} = r_{ip3} \times ADP - \frac{IP_3{}^{ADP}}{\tau_{ip3}} \tag{1}$$

where $IP_3{}^{ADP}$ is the quantity of IP_3 produced by the PLC pathway within the cytoplasm, and r_{ip} and τ_{ip3} are respectively the production and decay rates of $IP_3{}^{ADP}$.

Hydrolysis of membrane lipid phosphatidylinositol 4, 5–bisphosphate (PIP_2) through phosphoinositide-specific phospholipase C (PLC) can increase the level of IP_3. This behaviour and its activation rate are also modulated by $[Ca^{2+}]_i$ and can be modelled through PLC_δ signalling (De Pittà, Goldberg, Volman, Berry, & Ben-Jacob, 2009) as

$$PLC_\delta = PLC_{\delta'} \times Hill\left([Ca^{2+}_{P2Y}]_i, 2, K_{PLC_\delta}\right) \tag{2}$$

where the maximum IP_3 production (De Pittà et al., 2009), which depends on PLC_δ, is given by

$$PLC_{\delta'} = \frac{\overline{PLC_{\delta'}}}{1 + \frac{IP_3}{K_\delta}} \tag{3}$$

K_δ is the inhibition constant of the PLC_δ activity. The standard Hill function has been used in Eq. 3 formulated by

$$Hill(x, n, K) \equiv \frac{x^n}{x^n + K^n} \tag{4}$$

where x is the substance in question. n and K are respectively the Hill coefficient and the midpoint of the Hill function at which the magnitude of the function becomes one-half.

IP_3 is mainly degraded through phosphorylation into inositol 1, 3, 4, 5-tetrakisphosphate (IP_4) which is catalysed by IP_3 3-kinase (3K) and regulated by $[Ca^{2+}]_i$ in a complicated manner. It is also dephosphorylated by inositol polyphosphate 5-phosphatase (5P). The degradation rate of IP_3 by these two events (De Pittà et al., 2009) is modelled as

$$IP_3{}^{5p} \approx \bar{r}_{5p} \times IP_3 \tag{5}$$

$$IP_3{}^{3K} = \bar{v}_{3K} \times Hill([Ca^{2+}_{P2Y}]_i, 4, K_D) \times Hill(IP_3, 1, K_3) \tag{6}$$

where $\bar{r}_{5p}$ is the rate of IP_3 degradation associated with IP-5p. $\bar{v}_{3K}$ is the maximum rate of degradation by $IP3^{3K}$. K_D and K_3 are short for $[Ca^{2+}]_i$ and IP_3 affinities of $IP_3{}^{3K}$ for the two Hill functions.

Finally, the rate at which IP_3 changes with respect to time is described in terms of an ODE given by

$$\frac{dIP_3}{dt} = {IP_3}^{ADP} + PLC\delta - {IP_3}^{5p} - {IP_3}^{3K} \quad (7)$$

To overcome the limitations of existing IP_3R models (De Young & Keizer, 1992; Gabbiani & Cox, 2017; Li & Rinzel, 1994; Sneyd & Dufour, 2002) in their inability to capture human Ca^{2+} data for microglia as also encountered for human microglial P2X receptors reported in (Poshtkohi et al., 2021), we propose a new IP_3 receptor model using four state variables similar to (Poshtkohi et al., 2021) as shown in Fig 2. In the model, the channel states of *desensitisation*, *sensitisation*, *open* and *closed* are represented by *D*, *S*, *O* and *C* respectively. The model assumes that IP_3R has a low open probability), namely, the C/S/O path (note that in this state the forward S/O path has a low kinetic rate about 100 times lower than when the channel fully opens). Then, Ca^{2+} releases and binds to intracellular Ca^{2+} binding sites on the receptor. This switches the IP_3R to an open state with high open probability (the path from S to O).

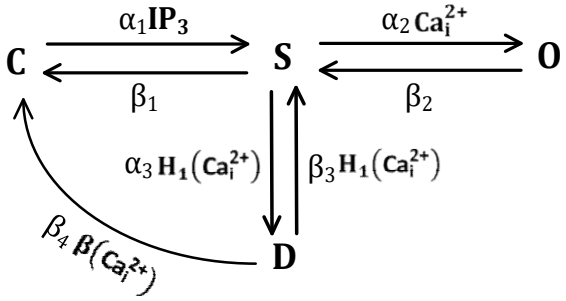

Figure 2: A reaction network developed to capture the Ca^{2+} current passing through the Ca^{2+}-gated IP_3 receptor on the ER lumen in human microglia. The states *D*, *S*, *O* and *C* respectively stand for *desensitisation*, *sensitisation*, *open* and *closed*. It is assumed that IP_3 has

to bind to its binding site before Ca^{2+} is able to bind and the receptor can open. H_1 and β functions are defined in Eqs. 12-13.

As cytosolic Ca^{2+} reaches very high levels, the IP_3R switches to an inactivated state through the complex paths of O/S and S/D. Therefore, the gating properties of the IP_3 receptor are divided into four individual states, including, activation (S to O) and sensitization (C to S), desensitisation (full-duplex Ca^{2+}-gated transition between S and D) and deactivation (mainly from D to C and partly from O to S and then C). Activation is a quick process (it happens after the receptor is sensitised by IP_3) over which the receptor opens and Ca^{2+} is released from the ER lumen to the cytosol (CICR). The CICR state is modelled in the transition from S to O. The receptor is fully activated when IP_3 binds through the transition between states C and S, and Ca^{2+} gates the receptor through state S to O.

As shown later (Fig 3(a)), microglial human P2Y-mediated Ca^{2+} response has three significant phases at the macroscopic level: A to B (CICR), B to C (desensitisation), and C to D (deactivation). The system of time-dependent differential equations formed by the reaction network in Fig 2 is modelled in Eqs. 8-11 by directly applying the law of mass action. These equations describe the rate at which the model states change in the time domain. Each state C, S, D or O corresponds to the fraction of time IP_3R remains in any state.

$$\frac{dC}{dt} = \beta_1 S + \beta_4 \mathrm{H}_1([\mathrm{Ca}^{2+}_{\mathrm{P2Y}}]_i)D - \alpha_1[IP_3]C \tag{8}$$

$$\frac{dS}{dt} = \alpha_1[IP_3]C + \beta_2 O + \beta_3 \mathrm{H}_1([\mathrm{Ca}^{2+}_{\mathrm{P2Y}}]_i)D - (\alpha_2[\mathrm{Ca}^{2+}_{\mathrm{P2Y}}]_i + \alpha_3 \mathrm{H}_1([\mathrm{Ca}^{2+}_{\mathrm{P2Y}}]_i) + \beta_1)S \tag{9}$$

$$\frac{dD}{dt} = \alpha_3 H_1([\mathrm{Ca}^{2+}_{\mathrm{P2Y}}]_i)S - \beta_3 \mathrm{H}_1([\mathrm{Ca}^{2+}_{\mathrm{P2Y}}]_i)D - \beta_4 \beta([\mathrm{Ca}^{2+}_{\mathrm{P2Y}}]_i)D \quad (10)$$

$$\frac{dO}{dt} = \alpha_2 [\mathrm{Ca}^{2+}_{\mathrm{P2Y}}]_i S - \beta_2 O \quad (11)$$

where the set of α and β parameters are forward and reverse reaction rates for the IP_3R model. The function H_1 is a first-order (*n=1*) version of the standard *Hill* function defined in Eq. 12 for human microglia as follows

$$\mathrm{H}_1([\mathrm{Ca}^{2+}_{\mathrm{P2Y}}]_i) = Hill([\mathrm{Ca}^{2+}_{\mathrm{P2Y}}]_i, n, K_S) \quad (12)$$

and the function β is defined using an exponential kinetic rate in Eq. 13 similar to the approach of the Hodgkin–Huxley (HH) model (Hodgkin & Huxley, 1952)—note that the HH model benefits from voltage-gated exponential rates while the model herein uses Ca^{2+}-gated exponential rate. In fact, this equation ensures that the *D* state goes back to its resting state when Ca^{2+} approaches its baseline (such a choice is more detailed in (Poshtkohi et al., 2021)).

$$\beta([Ca_i^{2+}]) \equiv e^{-\frac{[\mathrm{Ca}^{2+}_{\mathrm{P2Y}}]_i - a}{b}} \quad (13)$$

where *a* and *b* are calcium fitting levels.

In accordance with the HH model (Hodgkin & Huxley, 1952), CICR is modelled as two identical activation gates (which open with the probability of *O*) and a single inactivation gate (which is activated by a probability of *h*). So, the channel dynamics are assumed to be affected by these two gates. At resting microglia, the *h* gate is open whereas the *O* gates are closed, thus the entire IP_3R is closed. When IP_3 gates the receptor in Fig 2, the *O* gates are

quickly activated and in turn, the h gate closes. Since it is expected that these two gates work in tandem, the resultant probability that describes the receptor dynamics is obtained by multiplying the probability of the gates together. The D state is indicative of inactivation in the model, so the equation for probability h is given as

$$h = 1 - D \tag{14}$$

A typical h transient can be seen in Fig 3(b). The Ca^{2+} flux through the IP_3R in accordance with the HH formalism (Hodgkin & Huxley, 1952) can be mathematically written as

$$J_{IP_3R} = \alpha_4 \times h \times O^3 \times (C_0 - (1 + C_1) \times [\mathrm{Ca}^{2+}_{\mathrm{P2Y}}]_i) \tag{15}$$

where α_4 is the maximal rate of Ca^{2+} release from the IP_3 receptor, C_0 is the free intracellular Ca^{2+} concentration (Wade, McDaid, Harkin, Crunelli, & Kelso, 2012) and C_1 is the ER lumen to cytoplasm volume ratio (Wade et al., 2012). It is worth noting that activation and inactivation of the model are dependent on IP_3 and Ca^{2+} and h depends on the activation gates in contrast to the HH model (where they are independent).

The flow of Ca^{2+} ions through the leak channel is modelled using a simple linear equation as

$$J_{Leak} = \alpha_5 \times (C_0 - (1 + C_1) \times [\mathrm{Ca}^{2+}_{\mathrm{P2Y}}]_i) \tag{16}$$

where α_5 is the Ca^{2+} leakage rate.

The SECRA pump is described by the Michaelis-Menten kinetics (Silva, Kapela, & Tsoukias, 2007), as

$$J_{SECRA} = \bar{J}_{SECRA} \frac{[\mathrm{Ca}^{2+}_{\mathrm{P2Y}}]_i^{\,2}}{K_{SECRA}^{\,2} + [\mathrm{Ca}^{2+}_{\mathrm{P2Y}}]_i^{\,2}} \tag{17}$$

Ca^{2+} signalling is formulated as a fluid compartment model, which we assume is well mixed. We describe the changes in Ca^{2+} concentrations in the cytosolic region as

$$\frac{d[\mathrm{Ca}^{2+}_{\mathrm{P2Y}}]_i}{dt} = J_{IP3R} + J_{Leak} - J_{SECRA} \tag{18}$$

2. 2. Total Ca^{2+} Model

In Fig. 1, we introduced two sources of intercellular Ca^{2+}. A major source is mediated from the internal stores activated by the $P2Y_{12}$ receptor and via P2XR receptors located on the tip of the microglia's process. Therefore, it is expected the total Ca^{2+} profile can be approximated by aggregating these two sources. However, diffusion from the process will involve a time delay which is modelled as a linear diffusion equation (Goldberg, De Pittà, Volman, Berry, & Ben-Jacob, 2010; Naeem, McDaid, Harkin, Wade, & Marsland, 2015). Consequently, the total time-dependant calcium concentration in the soma $[\mathrm{Ca}^{2+}_{\mathrm{tot}}(t)]$ is modelled as

$$\mathrm{Ca}^{2+}_{\mathrm{tot}}(t) = [\mathrm{Ca}^{2+}_{\mathrm{P2Y}}(t)] + \alpha \times [\mathrm{Ca}^{2+}_{\mathrm{P2X}}(t - t_d)] \tag{19}$$

where α is a Ca^{2+} scaling factor and t_d models the time delay that P2X-mediated Ca^{2+} takes to travel the length of the process to the soma. The first term on the right of Eq. 19 is found in the solution Eq. 18. To obtain the numerical values for $\mathrm{Ca}^{2+}_{\mathrm{P2X}}(t)$, it is required to solve a system of ODEs comprised of eleven state variables modelled in (Poshtkohi et al., 2021) (see supplementary material (S2) for this model). We wish to point out that α requires to have a value greater than one if the model is to capture the second peak in the pAkt experimental

data. This is likely because the density of P2X receptors is upregulated (Tsuda et al., 2009) when microglia are activated.

2. 3. CaMKII Model

The mathematical model used for CaMKII is adopted from (Hund et al., 2008) and is given by Eqs. 21-23. In contrast to (Hund et al., 2008), the order of the hill function is raised to the power of two which allows the model to better capture the experimental data.

$$CaMK_{bound} = CaMK_0 \times (1 - CaMK_{trap}) \times Hill^2([Ca_i^{2+}]_{tot}, 1, K_{m,CaM}) \quad (21)$$

$$CaMK_{active} = CaMK_{bound} + CaMK_{trap} \quad (22)$$

$$\frac{dCaMK_{trap}}{dt} = \alpha_{CaMK} \times CaMK_{bound} \times CaMK_{active} - \beta_{CaMK} \times CaMK_{trap} \quad (23)$$

where $CaMK_{active}$, $CaMK_{bound}$ and $CaMK_{trap}$ are the fractions of active, bound and trapped CaMKII subunits, $CaMK_0$ is this fraction at equilibrium, and α_{CaMK} and β_{CaMK} are respectively phosphorylation and dephosphorylation rates of CaMKII (Hund et al., 2008; Hund & Rudy, 2004).

2. 4. PI3K/AKT Model

With reference to the reaction network in Table 1 (which is inspired by and adapted from (Hatakeyama et al., 2003; Tan et al., 2013)), reactions 1 and 2 given in Table 1 involve the PI3K enzyme phosphorylates PIP_2, (producing PIP_3), followed by dephosphorylation of PIP_3 to PIP_2 through PTEN. In these reactions, the PI3K enzyme is assumed to be directly activated by CaMKII. Thus, the first reaction has a variable forward rate controlled by CaM activity which is defined using Eq. 24 as

$$CaM = CaMK_{active} \quad (24)$$

In the next stage, the phosphorylation of Akt to pAkt is carried out by the PIP3 enzyme, as shown in reaction 3. pAkt is dephosphorylated back to Akt by the PP2A enzyme in reaction 4. Finally, in the third stage, PDK1 acts as a major potentiator of Akt given by reactions 5 to 8. Since the activity of PDK1 in Fig. 1 relies on both PIP3 and Akt, we exploit a slightly generalised variant of Michaelis-Menten kinetics in order for the model to capture this complex behaviour. The first step of the enzymatic kinetics due to PDK1 is divided into two phases. The first is an activated form of PDK1 by PIP_3 described by reaction 5. It is possible that PDK1 also interacts with the PIP3-Akt compound produced by reaction 3, which is expressed by reaction 5 and forms PIP_3-PDK1-Akt (which is also affected by reaction 7). Then, the new complex PIP_3-PDK1 phosphorylates Akt, and one original reactant is reproduced leaving pAkt as a final product which contributes to a higher level of pAkt in tandem with reaction 3. PIP3-PDK1 is then disassociated with PIP3 and PDK is given by reaction 5.

Table 1: CaMKII-mediated PI3K/Akt reaction network developed for microglia (inspired by and adapted from (Hatakeyama et al., 2003; Tan et al., 2013)).

Num.	Reaction
PIP_2 phosphorylation and PIP_3 inhibition by PTEN	
1	$\underbrace{\text{PIP}_2}_{x_1} + \underbrace{\text{PI3K}}_{x_2} \underset{b_1}{\overset{a_1 \times CaM}{\rightleftarrows}} \underbrace{\text{PIP}_2\text{-PI3k}}_{y_1} \xrightarrow{c_1} \underbrace{\text{PIP}_3}_{x_3} + \underbrace{\text{PI3K}}_{x_3}$
2	$\underbrace{\text{PIP}_3}_{x_3} + \underbrace{\text{PTEN}}_{x_4} \underset{b_2}{\overset{a_2}{\rightleftarrows}} \underbrace{\text{PIP}_3\text{-PTEN}}_{y_2} \xrightarrow{c_2} \underbrace{\text{PIP}_2}_{x_1} + \underbrace{\text{PTEN}}_{x_4}$
Akt phosphorylation and pAkt inhibition by PP2A	
3	$\underbrace{\text{PIP}_3}_{x_3} + \underbrace{\text{Akt}}_{x_5} \underset{b_3}{\overset{a_3}{\rightleftarrows}} \underbrace{\text{PIP}_3\text{-Akt}}_{y_3} \xrightarrow{c_3} \underbrace{\text{PIP}_3}_{x_3} + \underbrace{\text{pAkt}}_{x_6}$

4	$\underbrace{\text{pAkt}}_{x_6} + \underbrace{\text{PP2A}}_{x_7} \underset{b_4}{\overset{a_4}{\rightleftarrows}} \underbrace{\text{pAkt-PP2A}}_{y_4} \xrightarrow{c_4} \underbrace{\text{PP2A}}_{x_7} + \underbrace{\text{Akt}}_{x_5}$
pAkt potentiation by PDK1	
5	$\underbrace{\text{PIP}_3}_{x_3} + \underbrace{\text{PDK1}}_{x_8} \underset{b_5}{\overset{a_5}{\rightleftarrows}} \underbrace{\text{PIP}_3\text{-PDK1}}_{y_5}$
6	$\underbrace{\text{PIP}_3\text{-Akt}}_{y_3} + \underbrace{\text{PDK1}}_{x_8} \underset{b_6}{\overset{a_6}{\rightleftarrows}} \underbrace{\text{PIP}_3\text{-PDK1-Akt}}_{y_6}$
7	$\underbrace{\text{PIP}_3\text{-PDK1}}_{y_5} + \underbrace{\text{Akt}}_{x_5} \underset{b_7}{\overset{a_7}{\rightleftarrows}} \underbrace{\text{PIP}_3\text{-PDK1-Akt}}_{y_6} \xrightarrow{c_5} \underbrace{\text{pAkt}}_{x_6} + \underbrace{\text{PIP}_3\text{-PDK1}}_{y_5}$

To drive a mathematical model of the aforementioned reactions in terms of a system of ODEs, the law of mass action is employed. In Table 1, all species are denoted by either x_i or y_i to simplify writing the model equations. Consequently, the non-linear ODE Akt model is described by Eqs. 25-38 below

$$\frac{dx_1}{dt} = -a_1 \times CaM \times x_1 x_2 + b_1 y_1 + c_2 y_2 \quad (25)$$

$$\frac{dx_2}{dt} = -a_1 \times CaM \times x_1 x_2 + (b_1 + c_1) y_1 \quad (26)$$

$$\frac{dy_1}{dt} = a_1 \times CaM \times x_1 x_2 - (b_1 + c_1) y_1 \quad (27)$$

$$\frac{dx_3}{dt} = -a_2 x_3 x_4 + b_2 y_2 + c_1 y_1 - a_3 x_3 x_5 + (b_3 + c_3) y_3 - a_5 x_3 x_8 + b_5 y_5 \quad (28)$$

$$\frac{dx_4}{dt} = -a_2 x_3 x_4 + (b_2 + c_2) y_2 \quad (29)$$

$$\frac{dy_2}{dt} = a_2 x_3 x_4 - (b_2 + c_2) y_2 \quad (30)$$

$$\frac{dx_5}{dt} = -a_3 x_3 x_5 + b_3 y_3 + c_4 y_4 - a_7 y_5 x_5 + b_7 y_6 \quad (31)$$

$$\frac{dx_6}{dt} = -a_4 x_6 x_7 + b_4 y_4 + c_3 y_3 + c_5 y_6 \quad (32)$$

$$\frac{dy_3}{dt} = a_3 x_3 x_5 - (b_3 + c_3) y_3 - a_6 y_3 x_8 + b_6 y_6 \quad (33)$$

$$\frac{dx_7}{dt} = -a_4 x_6 x_7 + (b_4 + c_4) y_4 \quad (34)$$

$$\frac{dy_4}{dt} = a_4 x_6 x_7 - (b_4 + c_4) y_4 \quad (35)$$

$$\frac{dx_8}{dt} = -a_5 x_3 x_8 + (b_5 + c_6) y_5 - a_6 y_3 x_8 + b_6 y_6 \quad (36)$$

$$\frac{dy_5}{dt} = a_5 x_3 x_8 - a_7 y_5 x_5 + (b_7 + c_5) y_6 - b_5 y_5 \quad (37)$$

$$\frac{dy_6}{dt} = a_6 y_3 x_8 - (b_6 + b_7 + c_5) y_6 + a_7 y_5 x_5 \quad (38)$$

2. 5. Model Parameters Tuning

Parameter estimation is an inverse problem, where the parameters that cannot be directly determined are approximated to give the best fit to experimental data. An evolutionary strategy (Poshtkohi et al., 2021) was used to find the optimal values of the P2Y and PI3K/Akt model parameters that capture time-dependent kinetics. Parameters were fitted using an evolutionary optimiser where the aim is to reproduce the experimentally observed relationship between Ca^{2+} and pAkt dynamics and ADP stimulus magnitude and duration, as illustrated in Fig 3(a) and 4(a).

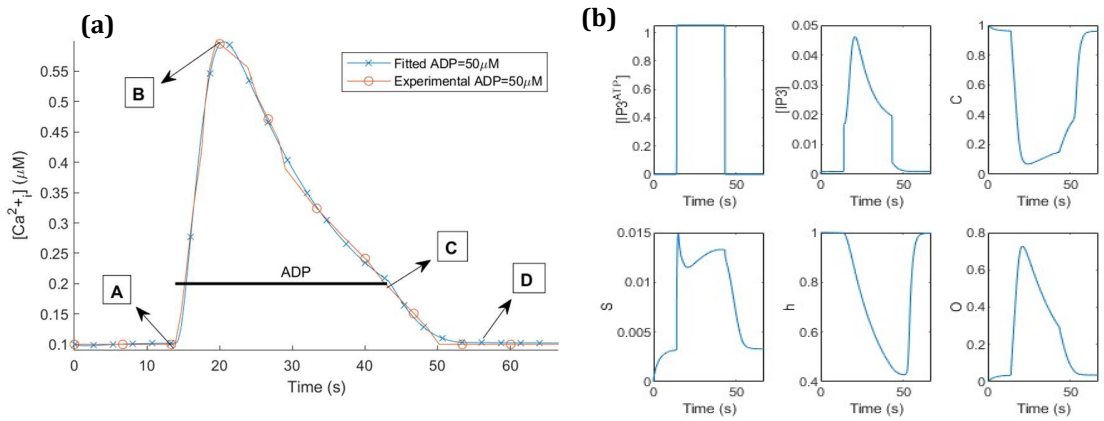

Figure 3: (a) Fitted intracellular Ca^{2+} upon an ADP treatment of 50μM within 29 seconds via activation of the $P2Y_{12}$ receptor in human microglia in comparison with experiments (Moore et al., 2015), and (b) transient responses of the state space to 50μM ADP for the $P2Y_{12}$ model in human microglia. These diagrams are derived from the response of the model to (a) by

numerical simulation. Note that (Moore et al., 2015) only provides calcium traces in relative fluorescence units and as there is no direct measurement for baseline and peak Ca^{2+} concentrations, they are approximated from the literature in (Sanada et al., 2002; Visentin, De Nuccio, & Bellenchi, 2006). Particularly, relative Ca^{2+} fluorescence from (Moore et al., 2015) was normalised and then rescaled to the values of concentrations reported in (Wang, Kim, Van Breemen, & McLarnon, 2000).

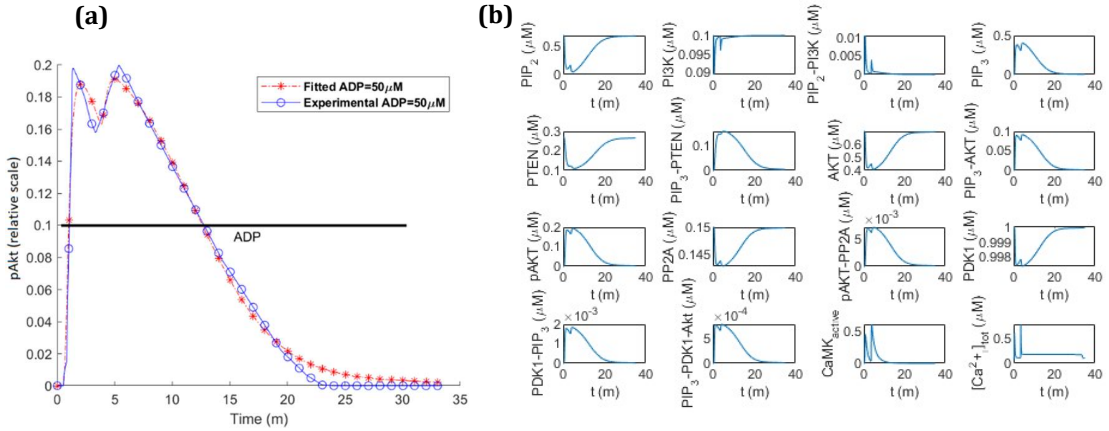

Figure 4: (a) Fitted pAkt levels upon an ADP exposure of 50μM within 30 minutes via activation of the $P2Y_{12}$ receptor in microglia, (b) transient responses of the state space to 50μM ADP for the PI3K/Akt model. Experimental data comes from (Irino et al., 2008). Note that the pAkt trace in (a) was obtained by interpolating five data points reported in (Irino et al., 2008) to a spline curve, where all data points were first normalised and then rescaled to a nominal value of 0.2 to show pAkt relative activity.

As can be seen in these figures, a good fit was obtained using the parameters given in Tables 2 and 3 for the Ca^{2+} and PI3K/Akt model. The P2Y model is crucial as it provides a method of addressing fundamental questions such as how calcium dynamics are governed

by the concentration of cytosolic IP_3, IP_3R density and state and also calcium uptake by calcium stores. The complete set of state changes in the model is shown in Figs 3(b) and 4(b).

Table 2: Parameters for the mathematical model and non-zero initial conditions of the P2Y-mediated calcium signalling in human microglia.

Parameter	Value	Unit	Description	Source
τ_{ip3}	0.0112	s^{-1}	IP3 degradation time constant	Fitted
r_{ip3}	1.872	$\mu M s^{-1}$	Rate of IP3 production	Fitted
K_{PLC_δ}	2.162	μM	Ca^{2+} affinity of PLC_δ	Fitted
$\overline{PLC_{\delta'}}$	29.197	$\mu M s^{-1}$	Maximal rate of IP3 production by PLC_δ	Fitted
K_δ	3.559	μM	Inhibition constant of PLCδ activity	Fitted
$\bar{r}_{5p}$	67.051	s^{-1}	IP_3 degradation rate by IP_3-5P	Fitted
$\bar{v}_{3K}$	745	$\mu M s^{-1}$	Maximum degradation rate by IP3-3K	Fitted
K_D	62.738	μM	Ca^{2+} affinity of IP_3-3K	Fitted
K_3	92.057	μM	IP_3 affinity of IP_3-3K	Fitted
α_1	14.771	$(\mu M)^{-1}s^{-1}$	Rate constant for C → S	Fitted
α_2	321	$(\mu M)^{-1}s^{-1}$	Rate constant for S → O	Fitted
α_3	7.485	s^{-1}	Outward rate constant for S → D	Fitted
α_4	2.686	s^{-1}	Maximal IP_3R rate	Fitted
α_5	0.0301	s^{-1}	Ca^{2+} leakage rate from ER	Fitted
β_1	3.501	s^{-1}	Rate constant for S → C	Fitted
β_2	3.034	s^{-1}	Rate constant for O → S	Fitted
β_3	1.5×10^{-5}	s^{-1}	Rate constant for D → S	Fitted
β_4	10	s^{-1}	Rate constant for D → C	Fitted
K_s	1	μM	Ca^{2+} affinity of H_1 function for IP_3R	Fitted
a	100×10^{-3}	μM	Coefficient of exponential β function for IP_3R	Fitted
b	1×10^{-3}	μM	Coefficient of exponential β function for IP_3R	Fitted
C_0	2	μM	Total free cytosol Ca^{2+} concentration	Fitted
C_1	0.185		Ratio of ER volume to cytosol volume	(Wade et al., 2012)
$\bar{J}_{SECRA}$	6.513	$\mu M s^{-1}$	Maximum SECRA current density	Fitted
K_{SECRA}	1.035	μM	Ca_i^{2+} for half activation of SERCA in IP_3 sensitive store	Fitted
$C\|_0$	1		Initial value of C	

$[Ca_i^{2+}]_0$	100×10^{-3}	μM	Initial Ca_i^{2+} concentration	(Zheng et al., 2015)

Table 3: Parameters and non-zero initial conditions of the total Ca^{2+}, CaMKII and PI3K/Akt models in microglia.

Parameter	Value	Unit	Description	Source
α	17.098		Ca^{2+} scaling factor	Fitted
t_d	3.228	m	Delay due to Ca^{2+} diffusion	Fitted
$CaMK_0$	26.229		Fraction of active CaMKII at equilibrium	Fitted
$K_{m,CaM}$	22.553	μM	Hill coefficient for CaMKII model	Fitted
α_{CaMK}	2223.93	m^{-1}	A rate of CaMKII	Fitted
β_{CaMK}	1.017	m^{-1}	A rate of CaMKII	Fitted
a_1	58.769	$(\mu M)^{-1}m^{-1}$	An association rate for PI3K pathway	Fitted
a_2	2.482	$(\mu M)^{-1}m^{-1}$	An association rate for PI3K pathway	Fitted
a_3	5.351	$(\mu M)^{-1}m^{-1}$	An association rate for PI3K pathway	Fitted
a_4	32.166	$(\mu M)^{-1}m^{-1}$	An association rate for PI3K pathway	Fitted
a_5	0.086	$(\mu M)^{-1}m^{-1}$	An association rate for PI3K pathway	Fitted
a_6	1.344	$(\mu M)^{-1}m^{-1}$	An association rate for PI3K pathway	Fitted
a_7	4.146	$(\mu M)^{-1}m^{-1}$	An association rate for PI3K pathway	Fitted
b_1	0.748	m^{-1}	A rate for activation of protein in PI3K pathway	Fitted
b_2	0.0045	m^{-1}	A rate for activation of protein in PI3K pathway	Fitted
b_3	1.046	m^{-1}	A rate for activation of protein in PI3K pathway	Fitted
b_4	14.084	m^{-1}	A rate for activation of protein in PI3K pathway	Fitted
b_5	82.187	m^{-1}	A rate for activation of protein in PI3K pathway	Fitted
b_6	8.0483	m^{-1}	A rate for activation of protein in PI3K pathway	Fitted
b_7	2.986	m^{-1}	A rate for activation of protein in PI3K pathway	Fitted
c_1	107.428	m^{-1}	A disassociation rate for PI3K pathway	Fitted
c_2	0.662	m^{-1}	A disassociation rate for PI3K pathway	Fitted
c_3	7.337	m^{-1}	A disassociation rate for PI3K pathway	Fitted

c_4	107.057	m^{-1}	A disassociation rate for PI3K pathway	Fitted
c_5	148.644	m^{-1}	A disassociation rate for PI3K pathway	Fitted
$[PIP_2]_0$	0.7	μM	Initial PIP_2 concentration	(Tan et al., 2013)
$[PI3K]_0$	0.1	μM	Initial PI3K concentration	(Tan et al., 2013)
$[PTEN]_0$	0.27	μM	Initial PTEN concentration	(Tan et al., 2013)
$[Akt]_0$	0.7	μM	Initial Akt concentration	(Tan et al., 2013)
$[PP2A]_0$	0.15	μM	Initial PP2A concentration	(Tan et al., 2013)
$[PDK1]_0$	1	μM	Initial PDK1 concentration	(Tan et al., 2013)

3. Results

The models were implemented in MATLAB Release 2022a. We used *ode23s* to numerically integrate the non-linear, stiff model equations with initial conditions and model parameters given in Tables 2 and 3, and (Poshtkohi et al., 2021) for the P2X receptor model (see supplementary material (S2)). The integration was carried out using the routine default MATLAB ODE solver timestep (because it uses dynamic step sizes for numerical integration) for a total of different time intervals to disclose fundamental patterns of Ca^{2+} and PI3K/Akt and dynamics.

3. 1. Human P2Y-mediated Ca^{2+} Dynamics

Fig 5 predicts $P2Y_{12}$ receptor mediates Ca^{2+} transient responses as a function of different ADP applications. The Ca^{2+} response shows that the Ca^{2+} curves rapidly increase in the presence of ADP followed by a steep decrease, particularly, for ADP levels greater than 20μM. When ADP is shortly applied at high concentrations for 2.5 seconds in Fig 5(a), a fast Ca^{2+} is

evoked but its amplitude is smaller than for wide exposure of ADP in comparison with all other cases. Ca^{2+} exchanges with Ca^{2+} stores involve IP_3R, SECRA and leak channel. Furthermore, when the IP_3R is activated, a relatively significant increase in $[Ca^{2+}]_i$ is observed in the cytosol which subsequently returns to its baseline level.

Fig 6 shows this behaviour where SECRA is mainly responsible for pumping Ca^{2+} back into the intracellular store. This kind of active homeostatic state is an illustration of the microglial function *in vivo* because if SECRA is inhibited then Ca^{2+} stores are depleted. $[Ca^{2+}]_i$ generally peaks within 4-7 seconds of ADP application. A typical theoretical time course of human IP_3 has been shown in Fig 3(b) where it reaches a maximum at approximately 6.8s after the application of ADP and the initial rise of Ca^{2+} and IP_3 follows the initial increase of IP_3^{ADP} which models activated GPCR levels. The desensitisation of the receptor gives rise to a fall in IP_3^{ADP}, IP_3 and Ca_i^{2+}on a timescale of seconds.

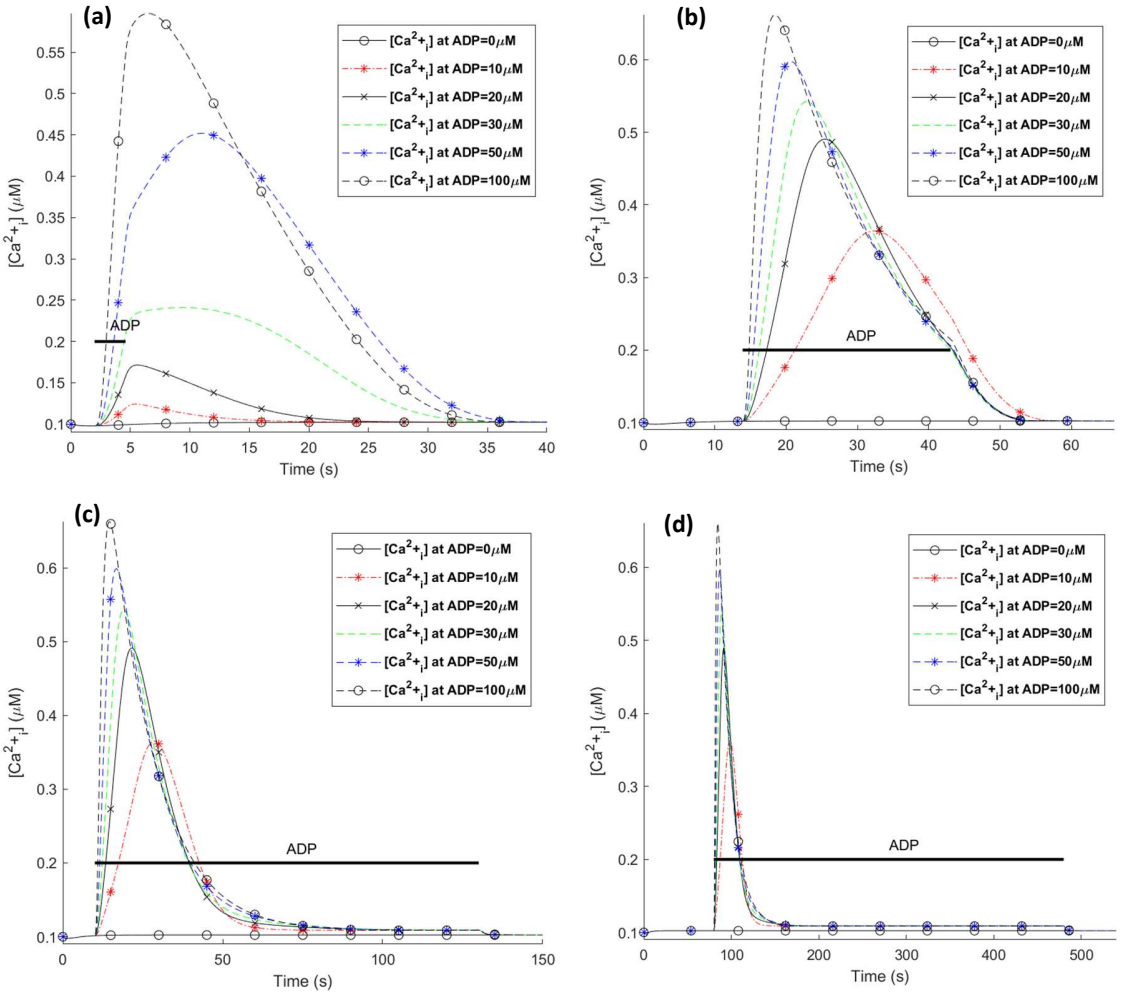

Figure 5: Prediction of different patterns in intracellular calcium transients upon different ADP pulse treatments within various time intervals (2.6, 30, 120 and 400 seconds respectively for figures a, b, c and d) via activation of the $P2Y_{12}$ receptor. Horizontal bars show the duration of ADP application that activates human microglial cells.

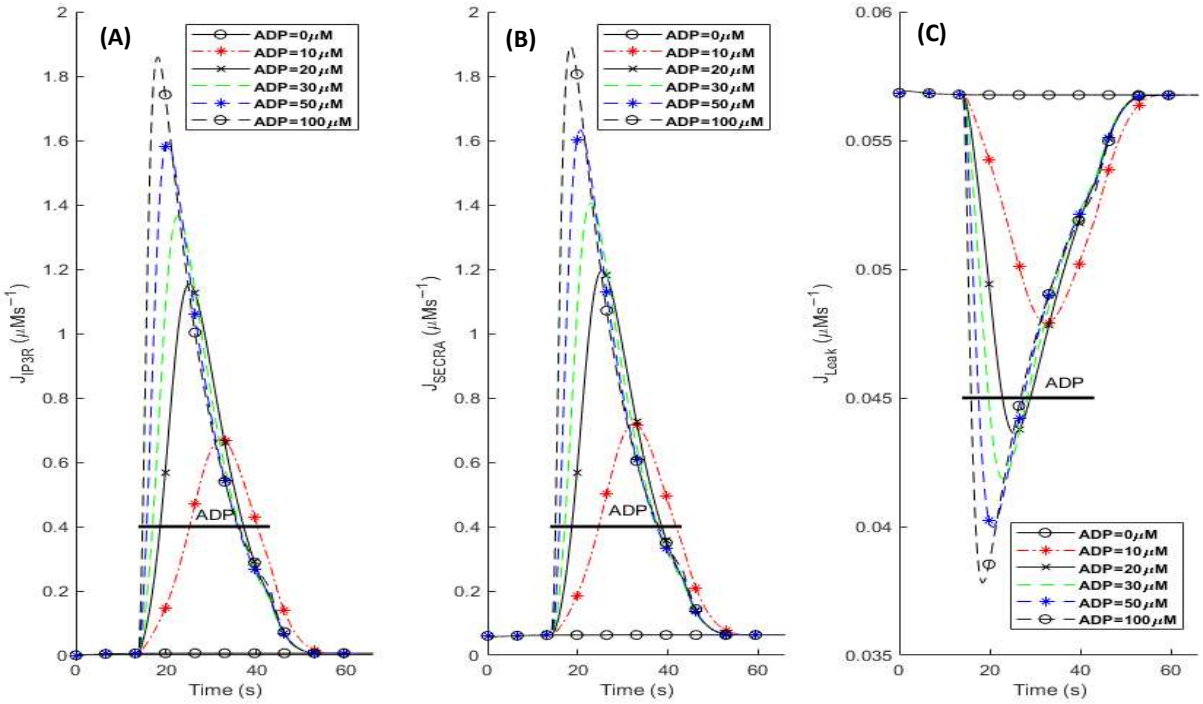

Figure 6: Estimation of current components for Fig 5(b) via 30-second ADP application. (A) Ca^{2+} flux through IP_3R enters the intracellular compartment. (B) Ca^{2+} flux that is pumped out by SECRA. (C) Ca^{2+} flux is due to the leak channel.

The different patterns of intracellular Ca^{2+} transients predicted for human microglial $P2Y_{12}$ receptors by different agonist concentrations and durations indicate that this receptor can regulate microglia activity based on changes in the brain microenvironment. More notably, the model successfully captures the dual requirement of preserving homeostasis while capable of providing a response when there is enough agonist concentration. Microglia must be sufficiently sensitive to their microenvironment to generate a response in case of an injury without being activated prematurely.

3. 2. PI3K/pAkt Pathway

The PI3K/pAkt model was activated by different concentrations of ADP to investigate the effect of its amplitude on the production of pAkt. Transient responses of total Ca^{2+} followed by increases in pAkt levels are shown in Fig 7. As Fig 7(a) results from the simultaneous activation of both $P2Y_{12}$ and P2X receptors, two Ca^{2+} peaks are observed where the first and second peaks correspond to $P2Y_{12}$ and P2X receptor activity respectively. The Ca^{2+} response of the $P2Y_{12}$ receptor rapidly falls off to baseline within a few minutes while the response to the P2X receptors gives rise to the second peak. Note that the Ca^{2+} does not fall off to baseline (and instead tends towards a plateau) after the second peak due to maintaining significant ionic currents in the presence of agonist (in contrast to the $P2Y_{12}$ receptor) by both P2X receptors as predicated in (Poshtkohi et al., 2021) and experimentally reported in (Yan et al., 2010). The corresponding pAkt activity is shown in Fig 7(b) as a function of ADP amplitude. For lower ADP levels, the amplitude of the first peak in the pAkt profile is significantly less than the second. Note that the first peak in Fig 7(b) aligns with the first Ca^{2+} spike in Fig 7(a), and the second Ca^{2+} peak reactivates the PI3K/pAkt pathway again to give rise to the second pAkt peak. As seen in the first Ca^{2+} spike of Fig 7(a), Ca^{2+} mediated by $P2Y_{12}$ is smaller than Ca^{2+} mediated by P2X receptors for lower ADP levels. In other words, because Ca^{2+} dynamics dictate the activation and regulation of the PI3K/Akt pathway, it is concluded that for high levels of ADP, both types of receptors participate equally in the activation of pAkt.

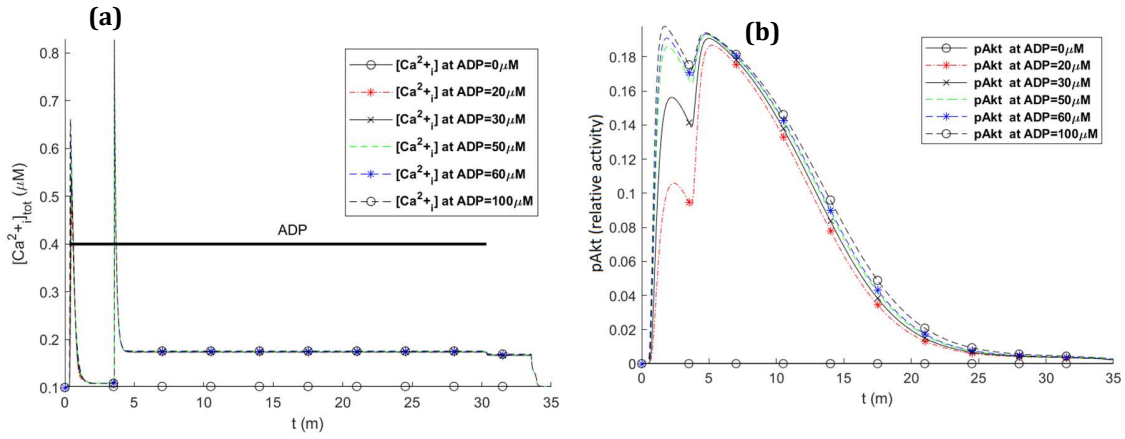

Figure 7: Prediction of different patterns in induced pAkt with respect to different ADP pulse treatments when $P2Y_{12}$ and P2X receptors are simultaneously activated in microglia.

While microglia spontaneous Ca^{2+} transients are less frequent than astrocytes in vivo (Brawek et al., 2017), it has been observed that the resting $[Ca^{2+}]_i$ in microglia is dynamically regulated through external factors (Hoffmann, Kann, Ohlemeyer, Hanisch, & Kettenmann, 2003). In vitro experiments indicate increases in $[Ca^{2+}]_i$ linked to LPS (lipopolysaccharide) stimulation, and microglia inflammatory responses (Hoffmann et al., 2003). This indicates the need to model these responses accurately to reflect microglia biology.

To understand how differential Ca^{2+} levels modulate pAkt dynamics, our model captures this upregulation by increasing 10% the density of the P2X receptors each time, as has been reported biologically (Choi, Ryu, Kim, & McLarnon, 2007). This results in a stepped increase in the Ca^{2+} influx which increases the $[Ca^{2+}]_i$ locally and therefore the diffusion gradient increases resulting in a larger Ca^{2+} current flow towards the microglia soma: in this approach, we model the stepped increase in diffusion by reducing the time delay associated with Ca^{2+} diffusion (time delay is defined as t_d in the model). To understand how this mechanism affects the pAkt responses, simulations were carried out while a periodic ADP

pulse protocol is used during which the conductance of P2X receptors is incremented by 10% (to model the increasing density of P2XRs) of its initial value and at the same time t_d is decremented by the same amount. As seen in Fig. 8, after six consecutive applications of ADP, the two peaks resulting from P2Y and P2X activity merge (see Fig. 8(b)) due to the stepped increase in the Ca^{2+} influx via the P2X receptor (see Fig. 8(a)).

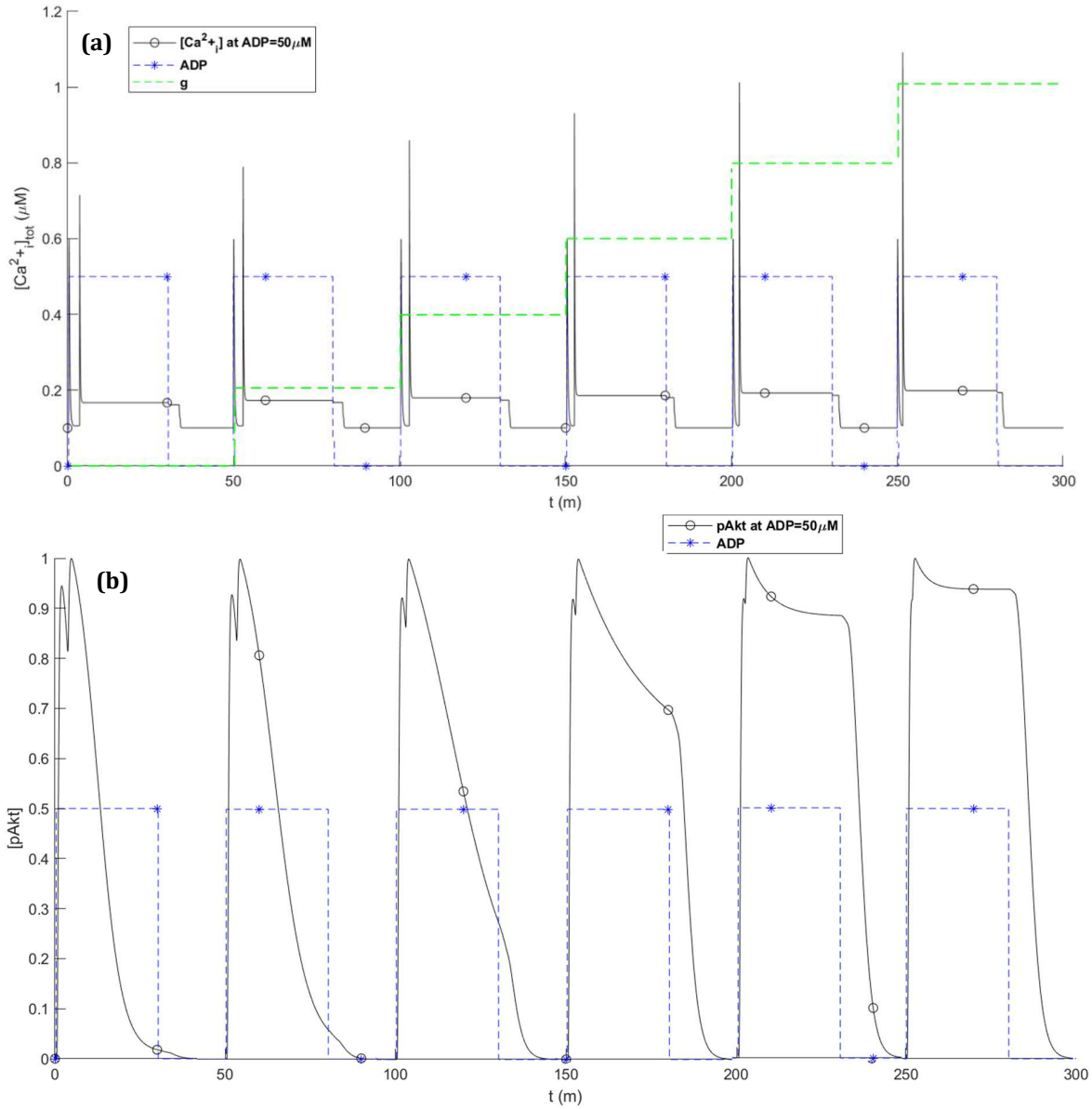

Figure 8: Simulation of the model when a repetitive ADP is applied, and on every rising edge of the ADP protocol, the conductance of P2X receptors is incremented by ten per cent and

the time delay due to Ca^{2+} diffusion is simultaneously decremented by ten per cent: (a) the total Ca^{2+} in the microglia soma, and (b) predicated pAkt levels. Note that the values of ADP, g and [pAkt] were normalised for illustrative purposes.

3. 3. Sensitivity Analysis of the Diffusion Model Parameters

As demonstrated throughout this paper two sources of $[Ca^{2+}]_i$ control the pAkt dynamics which can subsequently explain the experimentally reported biphasic transient responses in measuring pAkt levels. A linear diffusion equation with two parameters—including t_d and α—was then incorporated into the system to model the P2X-dependent source of Ca2+ moving from the process to the microglia soma. Because of the diffusion linearity, it was assumed that the effect of space (process length) is reflected in the diffusion time delay t_d. This was only aimed at showing upregulation of P2X receptors (α) and t_d (a representation of the effect of process length) can mathematically capture the pAkt data. The effect of space can be investigated using more complex spatial models as given in the Discussion section, however, this section carries out sensitivity analysis (SA) of the model diffusion parameters to elucidate the robustness of the model responses (Zi, 2011) and provide more information about the relationship between t_d and α.

The sensitivity analysis results can provide a detailed insight into the model parameters for future model refinements when new experimental data becomes available in order to develop more comprehensive models. Local sensitivity analysis (LSA) is used by which a single parameter (while others are kept constant) is varied and the effect of this perturbation is considered. This process is repeated for t_d and α. If y is a single response of a system of ODEs, LSA of this variable is defined (Zi, 2011) as

$$S_y = \frac{\partial y(t, p_i)}{\partial p_i} \tag{39}$$

where p_i denotes the *i*'th parameter. The partial derivative of y in Eq. 39 with respect to p_i can be approximated by using forward finite difference (FD) (Zi, 2011) as follows

$$\frac{\partial y(t, p_i)}{\partial p_i} \approx \frac{y(t, p_i + \Delta p_i) - y(t, p_i)}{\Delta p_i} \tag{40}$$

where Δp_i is a notation for a small change of the parameter p_i.

In general, when examining the robustness of sensitivity analysis, if the outcomes remain largely stable even after making slight perturbations to the model's fitted parameters, we can conclude that the sensitivity analysis is robust (Zi, 2011). For this study, the sensitivity analysis was carried out on the cytosolic pAkt concentration with respect to the t_d and α parameters of the PI3K/Akt models by stimulating the model under 50μM ADP. Fig. 9 illustrates a plot of Eq. 39 for parameter perturbations of 0.1%, 1% and 2%. As seen, SA results (A1 and B1) and responses of the model (A2 and B2) do not vary significantly, and graphs are similar; consequently, this verifies the sensitivity analysis robustness of the fitted model.

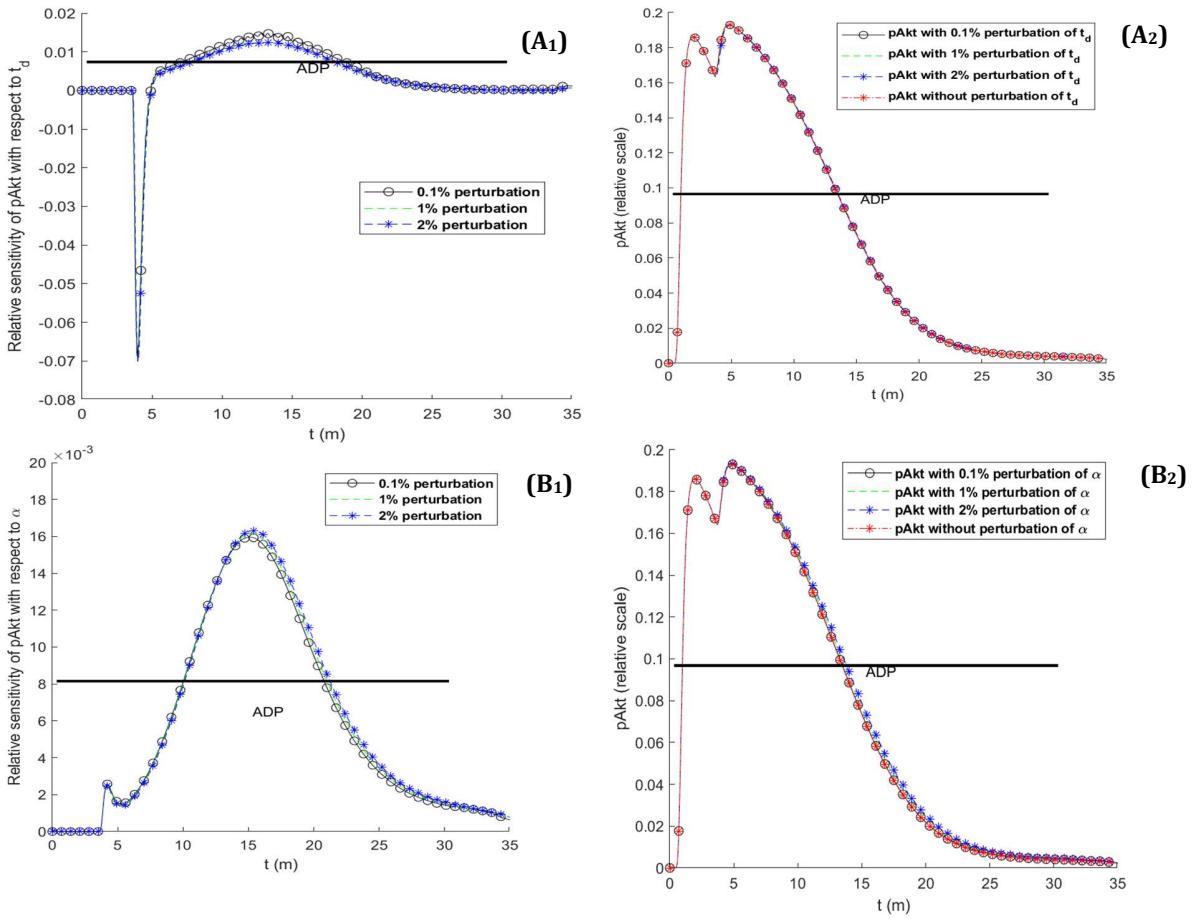

Figure 9: The sensitivity analysis of the intracellular pAkt for ADP=50μM with respect to t_d (see the top panel A) and α (see the bottom panel B). (A_1) and (B_1) show the relative sensitivities with 0.1%, 1% and 2% perturbation of the model parameters, namely, $\Delta p_i = 0.001 \times p_i$, $\Delta p_i = 0.01 \times p_i$ and $\Delta p_i = 0.02 \times p_i$. Horizontal bars show the duration of agonist exposure. The effects on the perturbed pAkt are illustrated in (A2) and (B2).

Finally, the effect of diffusion model parameters (t_d and α) on the pAkt response is considered as illustrated in Fig. 10. It indicates that the biphasic response of pAkt becomes monophasic when the value of α or t_d is halved (i.e., expression of P2XRs and diffusion due to space of the process plays a pivotal role in the hypothesis due to two individual sources of

$[Ca^{2+}]_i$). Increasing t_d (i.e., $\bar{t_d} > t_d$) and reducing α (i.e., $\bar{\alpha} < \alpha$) also removes the dual humps in pAkt.

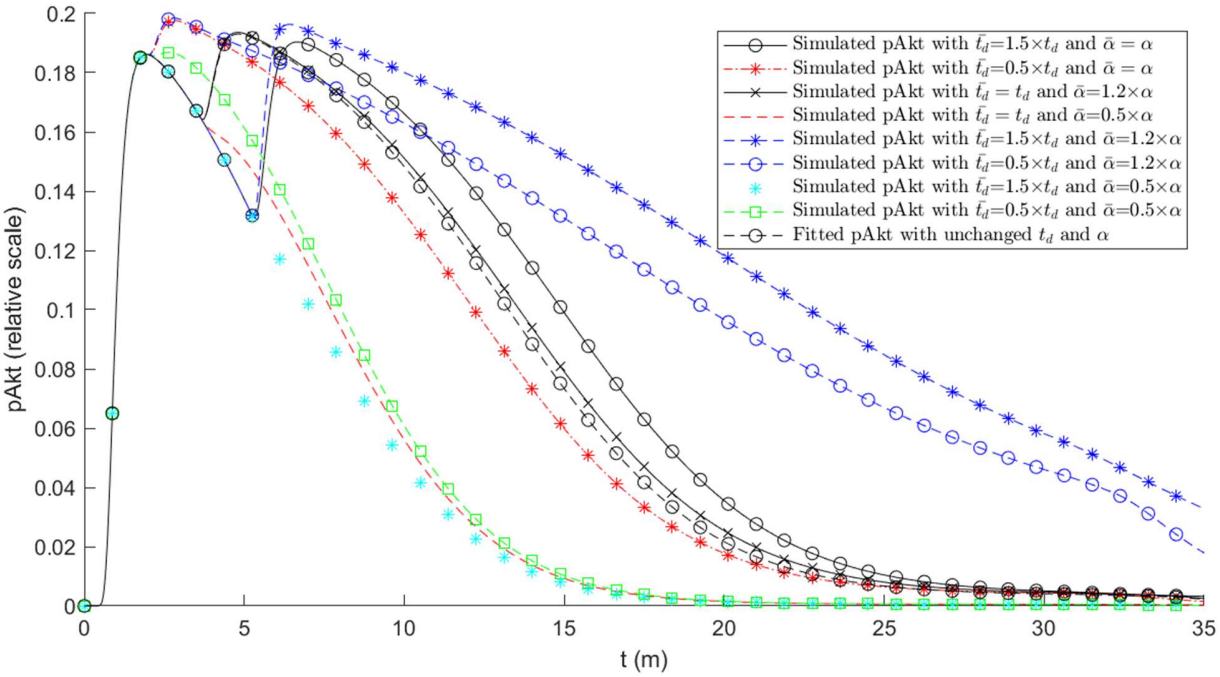

Figure 10: The effect of different combinations of diffusion model parameters (t_d and α) on the fitted pAkt response. Note that $\bar{t_d}$ and $\bar{\alpha}$ denote the unchanged, downscaled or upscaled version of their corresponding values, namely, t_d and α.

4. Discussion

Mathematical modelling of the PI3K/Akt pathway demonstrated changes in intracellular Ca^{2+} corresponding to changes in pAkt following extracellular ADP application. The hypothesis underpinning the proposed model was that Ca^{2+} influx due to both $P2Y_{12}$ and $P2X_{4/7}$ receptors actively stimulates the PI3K/Akt pathway which regulates pAkt. Moreover, the model was able to capture the experimentally observed biphasic response of the pAkt levels (Irino et al., 2008): the assumption being that cytosolic Ca^{2+} mediated by P2X receptors

must diffuse to the microglia soma before activating the PI3K/Akt pathway via CAMKII. It is important to capture these changes given the implications of dysregulated PI3K/Akt signalling cascade in microglia (Chu, Mychasiuk, Hibbs, & Semple, 2021).

$P2Y_{12}R$ substantially contributes to the intracellular Ca^{2+} by regulating the IP_3 receptor which resides on the ER region. This study constructed the first biophysical model of calcium dynamics in human microglia where a secondary messenger is activated by the $P2Y_{12}$ receptor. Specifically, a Markov model comprised of four state variables was proposed by modifying the base P2X model in (Poshtkohi et al., 2021) and changing its variable kinetic rates. In the IP_3R model, a first-order hill function was used in the transition between the sensitisation and desensitisation stages of the receptor, where all other rates were assumed to be constant or directly controlled by its ligand. We estimated the parameters of the model by the optimisation algorithm reported in (Poshtkohi et al., 2021). Even though experimental data for all species of the model except Ca^{2+} was unavailable, the model was able to capture the interplay between extracellular ADP, IP_3 and cytosolic Ca^{2+} dynamics.

Directed motility of microglia is driven by the elevation of intracellular Ca^{2+}, where the PI3K/Akt pathway is potentially involved in the polymerisation of the actin cytoskeleton. This research indicates two sources of $[Ca^{2+}]_i$ mediated by P2Y and P2X receptors, with a temporal dependency on influxes and changes in somatic Ca^{2+} levels. Subsequently, a comprehensive mathematical model of the PI3K/Akt pathway consisting of three major components—including, a superposition of P2Y-mediated Ca^{2+} and delayed P2X-mediated diffusion Ca^{2+}, CaMKII, and the main regulators of Akt phosphorylation. It was shown that a

minimum set of elements involved in the model was necessary to aid the parameter estimator in proving our hypothesis mathematically.

The simulation-based predictions in this article significantly contribute to our understanding of the physiology of microglia. The model architecture allowed a high degree of simplicity, accuracy, and predictability of P2YR-mediated changes in intracellular Ca^{2+} levels. Simulations show a rapid generation of IP_3 and activation of the IP_3 receptor mediated by the microglial human $P2Y_{12}$ receptor over a time scale of seconds. It was also shown that the $P2Y_{12}$-mediated response is significantly a function of ADP for its both duration and amplitude. For long applications of ADP, levels of $[Ca^{2+}]_i$ are independent of the duration but dependent on the amplitude; namely, the rise and fall of the response are very fast in a monotonic manner that completes in seconds and there is no basal-level plateau before ADP is removed as compared to rat microglial $P2Y_{12}$, and widely seen in other types of metabotropic receptors (e.g., $P2Y_2$ and $P2Y_6$ receptors) (Visentin et al., 2006). The hypothesis, that both P2X and P2Y receptors significantly modulate levels of Akt phosphorylation was also observable in all simulations. This work unveiled how changes in ADP concentration can create a biphasic response with distinct magnitudes.

Resting $[Ca^{2+}]_i$ for microglia have been reported in the nM range and can increase 3-fold upon stimulation (Umpierre et al., 2020), but is dependent on experimental set-up and stimuli used (Umpierre et al., 2020). The ability to alter these levels dynamically and in response to external stimuli is vital for the maintenance of brain physiology. It has been reported that the baseline $[Ca^{2+}]$ increases to facilitate nitric oxide and cytokine release in microglia (Färber & Kettenmann, 2006) and our model was used to understand how changes

in baseline [Ca^{2+}] affect the pAkt responses. A periodic ADP pulse protocol was applied where at each step increase in ADP the conductance of P2X receptors was incremented by 10% of its initial value while decreasing the time taken (by the same amount) for Ca^{2+} ions to reach the soma: upregulating P2XR causes a local increase in the [Ca^{2+}] and therefore a higher diffusion current and this was modelled by decreasing the time takes for Ca^{2+} ions to reach the soma. Model predictions show that after repeated ADP stimulation the biphasic response switches to a monophasic response as a result of P2Y and P2X activity merging due to the stepped increase in the Ca^{2+} influx via the P2X receptor. This data provides a rationale for the dynamic changes observed in the presence of inflammatory stimuli (Umpierre et al., 2020) and also proposes a link between the growing reports of human microglia heterogeneity and individual microglia Ca^{2+} responsiveness (Umpierre et al., 2020).

Microglial function depends upon complex signalling cascades involving a plethora of molecular entities. These cellular responses contribute to the measurable macroscopic features such as dynamic changes in intracellular Ca^{2+}. This complexity calls for a comprehensive biophysical model whose objective is to include many factors that affect the electrophysiology of microglia. This complexity is also reflected in the experimental data sets as mentioned in the paper. For instance, Ca^{2+} responses mediated by P2X receptors in (Hide et al., 2000) and phosphorylated Akt profile mediated by the $P2Y_{12}$ receptor reported in (Irino et al., 2008) have distinct Ca^{2+} profiles. Neither of these works tried to explain from where this intricacy originates. Mathematical modelling provides a robust methodology to integrate multiple components, develop hypotheses, and then arrange experiments in the laboratory to prove the theory. As already mentioned in the paper, several attempts have been made to develop models for the $P2Y_{12}R$/hIP_3R and PI3K/Akt pathway in other types of

cells except for human microglia. Due to the complexity and the increasing awareness of species differences (rodent microglia versus human microglia), microglia-specific human models were built specifically for the $hP2Y_{12}$ receptor in this article, and hP2X receptors in previous work (Poshtkohi et al., 2021) which was reused herein. Experimental microglia research provides raw data sets, however, there is often a lack of mechanistic examination to detail how intercellular and membrane-coupled components of microglia interact simultaneously. Most of these works show macroscopic properties of microglial activation by electrophysical or bioimaging measurements; therefore, important questions remain unanswered that mainly deal with explaining the molecular aspect of these cells. Existing human experimental models are very limited in providing insights into how microglia are modulated, however, the advent of iPSC technology will only increase datasets with relevance to human disease. To tackle this current issue, a model of PI3K/Akt was proposed for microglia that is simpler in contrast to very complex existing models (again developed for other type of cells except human microglia) but takes biological components specific to microglia and glial cells into account.

This article has added a considerable wealth of work to the physiology of microglia for which our developed mathematical tools have successfully provided profound biological information. The computational framework proposed here provides a primary basis that can be extended towards a better understanding of microglial activation, particularly *in vivo*. The model can also be refined as new experimental data become available. Although there remains a substantial body of theoretical and experimental work to be done in the scope of this research, there are further extensions to the base framework presented in this paper to assist neuroscientists. Several limitations within the model can direct improvements in

subsequent studies. The development of a more elaborate model for P2Y-mediated calcium signalling clearly calls for both kinetic and steady-state data of the PLC pathway and IP_3R channel by the neuroscience community. A major extension is to model potassium dynamics through $P2Y_{12}$ activation, which depends on protein kinase C (PKC), intracellular Ca^{2+} and membrane potential. This modelling requires building a new model of a channel that depends on these drivers. We hypothesise that an intermediate Markov model, similar to our IP_3R model that is gated by its key drivers, must be built from scratch. Other future work on extending the model proposed here can be the inclusion of distinct types of potassium (K^+) channels which are involved in functions such as proliferation and ramification, and voltage-gated sodium channels which have rapid kinetics and depend on membrane voltage (Kettenmann et al., 2011). Additionally, there is no model developed for microglia-specific aspects of voltage-gated sodium channels, ENT1, A_3, and A_{2A}, particularly using microglial human data (Kettenmann et al., 2011). Therefore, extensive research can be devoted to this channel and these receptors to further extend the biophysical models given in this research. Another limitation of the model is the omission of biological processes connecting ADP/ATP binding to cytokine responses. Within the model, a slower diffusion process takes place over an extended timescale. Consequently, it is possible to enhance the model by incorporating a more detailed mathematical representation of diffusion (Halnes, Østby, Pettersen, Omholt, & Einevoll, 2013). This enhanced description would better accommodate the spatiotemporal fluctuations in ion concentrations, specifically considering both intracellular Ca^{2+} sources stemming from P2Y and P2X receptors.

Supporting Information

S1 Text. The Effect of P2XR Absence on Model Dynamics. It shows that both $P2Y_{12}R$ and P2XRs must simultaneously be expressed by microglia to explain the twin peaks observed in the experimental pAkt data.

S2 Text. The mathematical model of P2X-mediated Ca^{2+} signalling in human microglia. It provides the equations and parameters of the P2X model (Poshtkohi et al., 2021) used in this article.

S3 Data. There are two data files that include raw data extracted from graphical experimental data sets presented in (Irino et al., 2008; Moore et al., 2015) for the P2Y receptor and PI3K/Akt pathway and used in the fitting process**.**

S4 Code. The MATLAB source codes of the entire model can be found on the GitHub page at https://github.com/poshtkohi/computational-neuroscience/tree/main/pi3k. It comes with a README file that explains the source code hierarchy.

References

Agell, N., Bachs, O., Rocamora, N., & Villalonga, P. (2002). Modulation of the Ras/Raf/MEK/ERK pathway by Ca2+, and calmodulin. *Cellular Signalling, 14*(8), 649-654.

Andrews, S., Stephens, L. R., & Hawkins, P. T. (2007). PI3K class IB pathway. *Science's STKE, 2007*(407), cm2-cm2.

Ashour, F., & Deuchars, J. (2004). Electron microscopic localisation of P2X4 receptor subunit immunoreactivity to pre-and post-synaptic neuronal elements and glial processes in the dorsal vagal complex of the rat. *Brain Research, 1026*(1), 44-55.

Brawek, B., & Garaschuk, O. (2013). Microglial calcium signaling in the adult, aged and diseased brain. *Cell Calcium, 53*(3), 159-169.

Brawek, B., Liang, Y., Savitska, D., Li, K., Fomin-Thunemann, N., Kovalchuk, Y., . . . Garaschuk, O. (2017). A new approach for ratiometric in vivo calcium imaging of microglia. *Scientific Reports, 7*(1), 6030.

Cattaneo, M. (2015). P2Y12 receptors: structure and function. *Journal of Thrombosis and Haemostasis, 13*, S10-S16.

Choi, H. B., Ryu, J. K., Kim, S. U., & McLarnon, J. G. (2007). Modulation of the purinergic P2X7 receptor attenuates lipopolysaccharide-mediated microglial activation and neuronal damage in inflamed brain. *Journal of Neuroscience, 27*(18), 4957-4968.

Chu, E., Mychasiuk, R., Hibbs, M. L., & Semple, B. D. (2021). Dysregulated phosphoinositide 3-kinase signaling in microglia: shaping chronic neuroinflammation. *Journal of Neuroinflammation, 18*, 1-17.

De Pittà, M., Goldberg, M., Volman, V., Berry, H., & Ben-Jacob, E. (2009). Glutamate regulation of calcium and IP 3 oscillating and pulsating dynamics in astrocytes. *Journal of biological physics, 35*(4), 383-411.

De Young, G. W., & Keizer, J. (1992). A single-pool inositol 1, 4, 5-trisphosphate-receptor-based model for agonist-stimulated oscillations in Ca2+ concentration. *Proceedings of the National Academy of Sciences, 89*(20), 9895-9899.

Dolan, A. T., & Diamond, S. L. (2014). Systems modeling of Ca2+ homeostasis and mobilization in platelets mediated by IP3 and store-operated Ca2+ entry. *Biophysical journal, 106*(9), 2049-2060.

Domercq, M., Vazquez, N., & Matute, C. (2013). Neurotransmitter signaling in the pathophysiology of microglia. *Frontiers in Cellular Neuroscience, 7*, 49.

Dorsam, R. T., & Kunapuli, S. P. (2004). Central role of the P2Y 12 receptor in platelet activation. *The Journal of clinical investigation, 113*(3), 340-345.

Erb, L., Woods, L. T., Khalafalla, M. G., & Weisman, G. A. (2019). Purinergic signaling in Alzheimer's disease. *Brain research bulletin, 151*, 25-37.

Fan, Y., Xie, L., & Chung, C. Y. (2017). Signaling pathways controlling microglia chemotaxis. *Molecules and cells, 40*(3), 163.

Färber, K., & Kettenmann, H. (2006). Functional role of calcium signals for microglial function. *Glia, 54*(7), 656-665.

Franco-Bocanegra, D. K., McAuley, C., Nicoll, J. A., & Boche, D. (2019). Molecular mechanisms of microglial motility: changes in ageing and Alzheimer's disease. *Cells, 8*(6), 639.

Gabbiani, F., & Cox, S. J. (2017). *Mathematics for neuroscientists*: Academic Press.

Goldberg, M., De Pittà, M., Volman, V., Berry, H., & Ben-Jacob, E. (2010). Nonlinear gap junctions enable long-distance propagation of pulsating calcium waves in astrocyte networks. *PLoS computational biology, 6*(8), e1000909.

Gurbel, P. A., Kuliopulos, A., & Tantry, U. S. (2015). G-protein–coupled receptors signaling pathways in new antiplatelet drug development. *Arteriosclerosis, thrombosis, and vascular biology, 35*(3), 500-512.

Halnes, G., Østby, I., Pettersen, K. H., Omholt, S. W., & Einevoll, G. T. (2013). Electrodiffusive model for astrocytic and neuronal ion concentration dynamics. *PLoS computational biology, 9*(12), e1003386.

Hatakeyama, M., Kimura, S., Naka, T., Kawasaki, T., Yumoto, N., Ichikawa, M., . . . Shirouzu, M. (2003). A computational model on the modulation of mitogen-activated protein kinase (MAPK) and Akt pathways in heregulin-induced ErbB signalling. *Biochemical Journal, 373*(2), 451-463.

Hickman, S., Izzy, S., Sen, P., Morsett, L., & El Khoury, J. (2018). Microglia in neurodegeneration. *Nature neuroscience, 21*(10), 1359-1369.

Hide, I., Tanaka, M., Inoue, A., Nakajima, K., Kohsaka, S., Inoue, K., & Nakata, Y. (2000). Extracellular ATP triggers tumor necrosis factor-α release from rat microglia. *Journal of neurochemistry, 75*(3), 965-972.

Hodgkin, A. L., & Huxley, A. F. (1952). A quantitative description of membrane current and its application to conduction and excitation in nerve. *The Journal of physiology, 117*(4), 500-544.

Hoffmann, A., Kann, O., Ohlemeyer, C., Hanisch, U.-K., & Kettenmann, H. (2003). Elevation of basal intracellular calcium as a central element in the activation of brain macrophages (microglia): suppression of receptor-evoked calcium signaling and control of release function. *Journal of Neuroscience, 23*(11), 4410-4419.

Honda, S., Sasaki, Y., Ohsawa, K., Imai, Y., Nakamura, Y., Inoue, K., & Kohsaka, S. (2001). Extracellular ATP or ADP induce chemotaxis of cultured microglia through Gi/o-coupled P2Y receptors. *Journal of Neuroscience, 21*(6), 1975-1982.

Hund, T. J., Decker, K. F., Kanter, E., Mohler, P. J., Boyden, P. A., Schuessler, R. B., . . . Rudy, Y. (2008). Role of activated CaMKII in abnormal calcium homeostasis and INa remodeling after myocardial infarction: insights from mathematical modeling. *Journal of Molecular and Cellular Cardiology, 45*(3), 420-428.

Hund, T. J., & Rudy, Y. (2004). Rate dependence and regulation of action potential and calcium transient in a canine cardiac ventricular cell model. *Circulation, 110*(20), 3168-3174.

Irino, Y., Nakamura, Y., Inoue, K., Kohsaka, S., & Ohsawa, K. (2008). Akt activation is involved in P2Y12 receptor-mediated chemotaxis of microglia. *Journal of neuroscience research, 86*(7), 1511-1519.

Jacques-Silva, M. C., Rodnight, R., Lenz, G., Liao, Z., Kong, Q., Tran, M., . . . Neary, J. T. (2004). P2X7 receptors stimulate AKT phosphorylation in astrocytes. *British journal of pharmacology, 141*(7), 1106-1117.

Ji, B., Bai, J., Mur, L. A., Zou, M., Han, J., Gao, R., & Yang, Q. (2020). Mathematical modelling of Her2 (ErbB2) PI3K/AKT signalling pathways during breast carcinogenesis to include PTPD2. *AIMS Mathematics, 5*(5), 4946-4958.

Jing, Z., Sui, X., Yao, J., Xie, J., Jiang, L., Zhou, Y., . . . Han, W. (2016). SKF-96365 activates cytoprotective autophagy to delay apoptosis in colorectal cancer cells through inhibition of the calcium/CaMKIIγ/AKT-mediated pathway. *Cancer Letters, 372*(2), 226-238.

Kettenmann, H., Hanisch, U.-K., Noda, M., & Verkhratsky, A. (2011). Physiology of microglia. *Physiological reviews, 91*(2), 461-553.

Koh, G., Teong, H. F. C., Clément, M.-V., Hsu, D., & Thiagarajan, P. (2006). A decompositional approach to parameter estimation in pathway modeling: a case study of the Akt and MAPK pathways and their crosstalk. *Bioinformatics, 22*(14), e271-e280.

Kölsch, V., Charest, P. G., & Firtel, R. A. (2008). The regulation of cell motility and chemotaxis by phospholipid signaling. *Journal of cell science, 121*(5), 551-559.

Koupenova, M., & Ravid, K. (2018). Biology of platelet purinergic receptors and implications for platelet heterogeneity. *Frontiers in pharmacology, 9*, 37.

Lemon, G. (2003). *Mathematical modelling of some aspects of intracellular second messenger signalling*: School of Mathematics and Statistics, Faculty of Science, University of Sydney.

Lemon, G., Gibson, W., & Bennett, M. (2003). Metabotropic receptor activation, desensitization and sequestration—I: modelling calcium and inositol 1, 4, 5-trisphosphate dynamics following receptor activation. *Journal of Theoretical Biology, 223*(1), 93-111.

Li, Y.-X., & Rinzel, J. (1994). Equations for InsP3 receptor-mediated [Ca2+] i oscillations derived from a detailed kinetic model: a Hodgkin-Huxley like formalism. *Journal of theoretical Biology, 166*(4), 461-473.

Madry, C., & Attwell, D. (2015). Receptors, ion channels, and signaling mechanisms underlying microglial dynamics. *Journal of Biological Chemistry, 290*(20), 12443-12450.

Mishra, J., & Bhalla, U. S. (2002). Simulations of inositol phosphate metabolism and its interaction with InsP3-mediated calcium release. *Biophysical Journal, 83*(3), 1298-1316.

Moore, C. S., Ase, A. R., Kinsara, A., Rao, V. T., Michell-Robinson, M., Leong, S. Y., . . . Bar-Or, A. (2015). P2Y12 expression and function in alternatively activated human microglia. *Neurology-Neuroimmunology Neuroinflammation, 2*(2).

Naeem, M., McDaid, L. J., Harkin, J., Wade, J. J., & Marsland, J. (2015). On the role of astroglial syncytia in self-repairing spiking neural networks. *IEEE Transactions on Neural Networks and Learning Systems, 26*(10), 2370-2380.

North, R. A. (2016). P2X receptors. *Philosophical Transactions of the Royal Society B: Biological Sciences, 371*(1700), 20150427.

Ohsawa, K., Irino, Y., Nakamura, Y., Akazawa, C., Inoue, K., & Kohsaka, S. (2007). Involvement of P2X4 and P2Y12 receptors in ATP-induced microglial chemotaxis. *Glia, 55*(6), 604-616.

Paolicelli, R. C., Sierra, A., Stevens, B., Tremblay, M.-E., Aguzzi, A., Ajami, B., . . . Bennett, M. (2022). Microglia states and nomenclature: A field at its crossroads. *Neuron, 110*(21), 3458-3483.

Pappalardo, F., Russo, G., Candido, S., Pennisi, M., Cavalieri, S., Motta, S., . . . Libra, M. (2016). Computational modeling of PI3K/AKT and MAPK signaling pathways in melanoma cancer. *PloS One, 11*(3), e0152104.

Poshtkohi, A., Wade, J., McDaid, L., Liu, J., Dallas, M., & Bithell, A. (2021). Mathematical modelling of human P2X-mediated plasma membrane electrophysiology and calcium dynamics in microglia. *PLOS Computational Biology, 17*(11), e1009520.

Purvis, J. E., Chatterjee, M. S., Brass, L. F., & Diamond, S. L. (2008). A molecular signaling model of platelet phosphoinositide and calcium regulation during homeostasis and P2Y12 activation. *Blood, The Journal of the American Society of Hematology, 112*(10), 4069-4079.

Sanada, M., Yasuda, H., Omatsu-Kanbe, M., Sango, K., Isono, T., Matsuura, H., & Kikkawa, R. (2002). Increase in intracellular Ca2+ and calcitonin gene-related peptide release through metabotropic P2Y receptors in rat dorsal root ganglion neurons. *Neuroscience, 111*(2), 413-422.

Sasaki, A. T., & Firtel, R. A. (2006). Regulation of chemotaxis by the orchestrated activation of Ras, PI3K, and TOR. *European journal of cell biology, 85*(9-10), 873-895.

Shakhidzhanov, S., Shaturny, V., Panteleev, M., & Sveshnikova, A. (2015). Modulation and pre-amplification of PAR1 signaling by ADP acting via the P2Y12 receptor during platelet

subpopulation formation. *Biochimica et Biophysica Acta (BBA)-General Subjects, 1850*(12), 2518-2529.
Silva, H. S., Kapela, A., & Tsoukias, N. M. (2007). A mathematical model of plasma membrane electrophysiology and calcium dynamics in vascular endothelial cells. *American Journal of Physiology-Cell Physiology, 293*(1), C277-C293.
Sneyd, J., & Dufour, J.-F. (2002). A dynamic model of the type-2 inositol trisphosphate receptor. *Proceedings of the National Academy of Sciences, 99*(4), 2398-2403.
Song, S. O., & Varner, J. (2009). Modeling and analysis of the molecular basis of pain in sensory neurons. *PloS One, 4*(9), e6758.
Tan, W. H., Popel, A. S., & Mac Gabhann, F. (2013). Computational model of Gab1/2-dependent VEGFR2 pathway to Akt activation. *PloS One, 8*(6), e67438.
Thei, L., Imm, J., Kaisis, E., Dallas, M. L., & Kerrigan, T. L. (2018). Microglia in alzheimer's disease: a role for ion channels. *Frontiers in neuroscience, 12*, 676.
Tsuda, M., Toyomitsu, E., Kometani, M., Tozaki-Saitoh, H., & Inoue, K. (2009). Mechanisms underlying fibronectin-induced up-regulation of P2X4R expression in microglia: distinct roles of PI3K–Akt and MEK–ERK signalling pathways. *Journal of cellular and molecular medicine, 13*(9b), 3251-3259.
Umpierre, A. D., Bystrom, L. L., Ying, Y., Liu, Y. U., Worrell, G., & Wu, L.-J. (2020). Microglial calcium signaling is attuned to neuronal activity in awake mice. *Elife, 9*, e56502.
Umpierre, A. D., Bystrom, L. L., Ying, Y., Liu, Y. U., & Wu, L.-J. (2019). Microglial Calcium Signaling is Attuned to Neuronal Activity. *bioRxiv*.
Visentin, S., De Nuccio, C., & Bellenchi, G. (2006). Different patterns of Ca 2+ signals are induced by low compared to high concentrations of P2Y agonists in microglia. *Purinergic signalling, 2*(4), 605.
Wade, J., McDaid, L. J., Harkin, J., Crunelli, V., & Kelso, S. (2012). Self-repair in a bidirectionally coupled astrocyte-neuron (AN) system based on retrograde signaling. *Frontiers in computational neuroscience, 6*, 76.
Wang, X., Kim, S., Van Breemen, C., & McLarnon, J. (2000). Activation of purinergic P2X receptors inhibits P2Y-mediated Ca2+ influx in human microglia. *Cell Calcium, 27*(4), 205-212.
Wolf, S. A., Boddeke, H., & Kettenmann, H. (2017). Microglia in physiology and disease. *Annual Review of Physiology, 79*, 619-643.
Yan, Z., Khadra, A., Li, S., Tomić, M., Sherman, A., & Stojilkovic, S. S. (2010). Experimental characterization and mathematical modeling of P2X7 receptor channel gating. *Journal of Neuroscience, 30*(42), 14213-14224.
Yano, S., Tokumitsu, H., & Soderling, T. R. (1998). Calcium promotes cell survival through CaM-K kinase activation of the protein-kinase-B pathway. *Nature, 396*(6711), 584-587.
Yegutkin, G. G. (2014). Enzymes involved in metabolism of extracellular nucleotides and nucleosides: functional implications and measurement of activities. *Critical reviews in biochemistry and molecular biology, 49*(6), 473-497.
Younger, D., Murugan, M., Rao, K. V. R., Wu, L.-J., & Chandra, N. (2019). Microglia receptors in animal models of traumatic brain injury. *Molecular neurobiology, 56*(7), 5202-5228.
Zheng, K., Bard, L., Reynolds, J. P., King, C., Jensen, T. P., Gourine, A. V., & Rusakov, D. A. (2015). Time-resolved imaging reveals heterogeneous landscapes of nanomolar Ca2+ in neurons and astroglia. *Neuron, 88*(2), 277-288.

Zi, Z. (2011). Sensitivity analysis approaches applied to systems biology models. *IET systems biology, 5*(6), 336-346.